Primordial black holes from Higgs inflation with a Gauss-Bonnet coupling

Ryodai Kawaguchi* and Shinji Tsujikawa†

Department of Physics, Waseda University, 3-4-1 Okubo, Shinjuku, Tokyo 169-8555, Japan

(Received 27 November 2022; accepted 14 February 2023; published 7 March 2023)

Primordial black holes (PBHs) can be the source for all or a part of today's dark matter density. Inflation provides a mechanism for generating the seeds of PBHs in the presence of a temporal period where the velocity of an inflaton field ϕ rapidly decreases toward 0. We compute the primordial power spectra of curvature perturbations generated during Gauss-Bonnet (GB) corrected Higgs inflation in which the inflaton field has not only a nonminimal coupling to gravity but also a GB coupling. For a scalar-GB coupling exhibiting a rapid change during inflation, we show that curvature perturbations are sufficiently enhanced by the appearance of an effective potential $V_{\rm eff}(\phi)$ containing the structures of plateau type, bump type, and their intermediate type. We find that there are parameter spaces in which PBHs can constitute all dark matter for these three types of $V_{\rm eff}(\phi)$. In particular, models with bump and intermediate types give rise to primordial scalar and tensor power spectra consistent with the recent Planck data on scales relevant to the observations of the cosmic microwave background. This property is attributed to the fact that the number of e-foldings ΔN_c acquired around the bump region of $V_{\rm eff}(\phi)$ can be as small as a few, in contrast to the plateau type, where ΔN_c typically exceeds the order of 10.

DOI: 10.1103/PhysRevD.107.063508

I. INTRODUCTION

If there were overdensity regions in the early Universe, primordial black holes (PBHs) may have formed as a result of the gravitational collapse during the radiation-dominated epoch [1–3]. Unlike astrophysical black holes, the PBHs can have a wide range of masses and can be the source for all or a part of dark matter (DM) [4,5] (see Refs. [6–13] for recent reviews). Although PBHs have not been observationally discovered yet, the detection of gravitational waves from binary black holes [14–17] has suggested a possibility that they may arise from nonstellar origins [18–21]. In addition, PBHs have been also considered as possible seeds of supermassive black holes in the centers of galaxies [22]. Various observations have given the upper limit to their abundance f as a function of mass M. In particular, the mass window in which all DM can be explained by PBHs exists in the range $10^{-16}M_\odot \lesssim M \lesssim 10^{-11}M_\odot$, where $M_\odot$ is a solar mass (see Ref. [23] for a recent study).

Inflation can provide a possible framework for generating the seed of PBHs on scales smaller than the observed cosmic microwave background (CMB) temperature anisotropies [24–83]. If there is an intermediate stage in which the velocity $\dot{\phi}$ of an inflaton field rapidly decreases toward 0 during inflation, it is possible to enhance curvature perturbations at particular scales. In the presence of an inflection point in the inflaton potential $V(\phi)$ around which the derivative $dV/d\phi$ is close to 0, the field velocity decreases as $\dot{\phi} \propto a^{-3}$ in the ultra-slow-roll (USR) regime, where a is a scale factor [44–46,48–51,53,56,69]. In many of these models, we require a tuning of model parameters to generate a plateau region of the potential. Moreover, if the number of e-foldings acquired in the USR regime exceeds the order 10, the scalar spectral index n_s on CMB scales tends to be inconsistent with the value constrained by the Planck data [84].

There are also models containing one or more bumps/dips or steps in the potential [57–59,68,72–75,80,81]. In this case, the scalar field rapidly loses its kinetic energy around them, resulting in a strong enhancement of curvature perturbations. It is also known that oscillating features can appear in the scalar power spectrum, especially for the step-type potential. One advantage of these models is that the number of e-foldings during transition can be as small as the order 1. This allows a possibility for the compatibility of models with the observed values of n_s and tensor-to-scalar ratio r. There are also multifield inflationary models leading to the enhancement of curvature perturbations at particular scales [25,27,29,38,39,47,66,67,70,71,82,83]. In this case, we need to address whether the presence of entropy perturbations does not contradict with CMB constraints on the isocurvature mode. The possibility for producing the seed of PBHs during preheating after inflation is also discussed in Refs. [85–88].

One of the advantages of PBHs as DM is that the origin of DM can be explained within the framework of the Standard Model (SM) of particle physics. A minimal model

*ryodai0602@fuji.waseda.jp
†tsujikawa@.waseda.jp

of inflation without introducing additional scalar degrees of freedom to those appearing in the SM is known as Higgs inflation, in which the Higgs field ϕ is nonminimally coupled to gravity [89–91] (see Refs. [92,93] for early related works). Indeed, this model is perfectly consistent with observational bounds on n_s and r constrained by the CMB data [94–98]. If we allow the runnings of Higgs self-coupling $\lambda(\phi)$ and nonminimal coupling $\xi(\phi)$, then it is possible to have an inflection point in the Higgs potential. This gives rise to a plateau region in which the enhancement of curvature perturbations occurs to generate the seed of PBHs [48,56,65,76]. In this scenario, the typical number of e-foldings acquired during the USR regime is of order 10, which results in the values of CMB observables deviating from those in standard Higgs inflation. The model can be consistent with the current CMB observations, but it is typically outside the 1σ contour constrained by the Planck data [48].

Recently, Kawai and Kim [77] proposed a single-field inflationary scenario in which the inflaton field is coupled to a Gauss-Bonnet (GB) curvature invariant $R^2_{\rm GB}$ of the form $\mu(\phi)R^2_{\rm GB}$. A scalar-field-dependent GB coupling $\mu(\phi)$ can give rise to an inflection point $\phi=\phi_c$ in an effective potential of the inflaton. On the other hand, we have to caution that a large contribution from the scalar-GB coupling to the inflaton energy density modifies the primordial scalar power spectrum on CMB scales [99–104]. Moreover, the scalar-GB coupling leads to propagation speeds of scalar and tensor perturbations different from the speed of light [105,106]. Since the Laplacian instabilities associated with negative squared propagation speeds may arise, we need to make sure that the stability conditions are not violated during inflation.

In Ref. [77], the scalar-GB coupling $\mu(\phi)=\mu_0\tanh[\mu_1(\phi-\phi_c)]$ was proposed to generate the seed of PBHs around the inflection point $\phi=\phi_c$. Since $\mu(\phi)$ approaches constants in the two asymptotic regimes $\phi\ll\phi_c$ and $\phi\gg\phi_c$, the scalar-GB coupling is important only in the vicinity of $\phi=\phi_c$. A temporal USR region can arise from the balance between the GB term and the scalar potential. The enhancement of curvature perturbations in such a transient epoch has been studied for natural inflation [77] and for the α attractor [78]. In these papers, the authors mostly focus on the USR regime realized by a plateau-type effective potential. In this case, the CMB observables are subject to modifications by the presence of a plateau region with a number of e-foldings of order 10. Hence, it is nontrivial to produce the large amplitude of primordial scalar perturbations responsible for the seed of PBHs, while satisfying CMB constraints on n_s and r.

In this paper, we will address this issue in Higgs inflation with a scalar-GB coupling as mentioned above. We will not incorporate the runnings of Higgs and nonminimal couplings to focus on effects of the scalar-GB coupling on the background and perturbations. We show that, besides the plateau-type effective potential, it is possible to realize a bump- or step-type effective potential. In this latter case, the field velocity $\dot{\phi}$ around $\phi=\phi_c$ decreases faster in comparison to the USR regime with a smaller number of e-foldings of order 1. The primordial scalar power spectrum can also have a sharp feature with a peak amplitude enhanced by a factor of 10^7. In such cases, PBHs can be the source for all DM in the mass range $10^{-16}M_\odot\lesssim M\lesssim 10^{-13}M_\odot$. Moreover, the bump-type effective potential can give rise to the values of n_s and r inside the 1σ observational contour constrained by the Planck CMB data. There are also intermediate-type potentials between plateau and bump types consistent with the CMB constraints, while generating the seed of PBHs. Thus, our inflationary scenario provides a versatile possibility for realizing various shapes of the effective scalar potential. We note that each shape of the potentials is discussed separately in different contexts in the literature.

This paper is organized as follows: In Sec. II, we obtain the background equations of motion in Higgs inflation with a scalar-GB coupling $\mu(\phi)R^2_{\rm GB}$ and revisit the scalar and tensor power spectra generated in slow-roll Higgs inflation with $\mu(\phi)=0$. In Sec. III, we derive an effective potential $V_{\rm eff}(\phi)$ of the inflaton field and classify it into three classes: (i) plateau-type, (ii) bump-type, and (iii) intermediate-type. In Sec. IV, we compute the primordial scalar power spectra for three sets of model parameters with which there are neither ghost nor Laplacian instabilities. We show that the bump type is favored over the plateau type for the consistency with CMB observables. In Sec. V, we calculate the PBH abundance relative to the relic DM density and show that our model produces a sufficient amount of PBHs that can be the source for all DM. Sec. VI is devoted to conclusions. Throughout the paper, we use the natural units ($c=\hbar=1$).

II. INFLATIONARY MODEL WITH A GAUSS-BONNET TERM

We begin with theories given by the action

$$\mathcal{S}=\int {\rm d}^4x\sqrt{-g}\left[\left(\frac{M_{\rm Pl}^2}{2}+\frac{1}{2}\xi\phi^2\right)R-\frac{1}{2}g^{\mu\nu}\nabla_\mu\phi\nabla_\nu\phi-V(\phi)+\mu(\phi)R^2_{\rm GB}\right], \tag{2.1}$$

where g is a determinant of the metric tensor $g_{\mu\nu}$, $M_{\rm Pl}$ is the reduced Planck mass, ξ is a nonminimal coupling constant, ϕ is a scalar field with the covariant derivative operator ∇_μ, and R is the Ricci scalar. The scalar field has a potential of the form

$$V(\phi)=\frac{\lambda}{4}\phi^4, \tag{2.2}$$

where λ is a positive coupling constant. The dynamics of nonminimally coupled inflation with the potential in Eq. (2.2) was originally addressed in Refs. [92,93] (see also Refs. [94,95,107–109]). It can also accommodate the Higgs potential $V(\phi)=\lambda(\phi^2-v^2)^2/4$ in the large-field regime $\phi^2 \gg v^2$, where $v=\mathcal{O}(10^2)$ GeV [89–91]. Provided that the nonminimal coupling is in the range

$$\xi \gg 1, \tag{2.3}$$

the self-coupling of order $\lambda = 0.01 \sim 0.1$ can be consistent with the amplitude of observed CMB temperature anisotropies.[1]

The scalar field is coupled to a GB curvature invariant defined by

$$R^2_{\rm GB} \equiv R^2 - 4R_{\mu\nu}R^{\mu\nu} + R_{\mu\nu\rho\sigma}R^{\mu\nu\rho\sigma}, \tag{2.4}$$

with a ϕ-dependent coupling function $\mu(\phi)$, where $R_{\mu\nu}$ and $R_{\mu\nu\rho\sigma}$ are the Ricci and Riemann tensors, respectively. The action in Eq. (2.1) belongs to a subclass of Horndeski theories with second-order field equations of motion [105,115–117] (see the Appendix). In this case, there is only one propagating scalar degree of freedom besides two tensor polarizations. As we will study in Sec. III, it is possible to enhance scalar perturbations at particular scales for a specific choice of $\mu(\phi)$. The action (2.1) corresponds to Higgs inflation corrected by the Higgs-GB coupling. This allows a possibility for generating the seed of PBHs as the source for all DM within the framework of the SM of particle physics.

We note that the $\xi \to 0$ limit in the action (2.1) with the potential of natural inflation corresponds to the model studied by Kawai and Kim [77]. In our model, the basic mechanism for the generation of seeds of PBHs is similar to that advocated in Ref. [77]. However, natural inflation is in tension with the observation of CMB temperature anisotropies [84]. Instead, we would like to construct an explicit inflationary model consistent with CMB observations, while enhancing curvature perturbations on scales relevant to PBHs. As we will show later, this is indeed possible for Higgs inflation with $\xi \gg 1$ in the presence of the scalar-GB coupling.

For the background, we consider a spatially flat Friedmann-Lemaître-Robertson-Walker (FLRW) line element given by

$$ds^2 = -dt^2 + a^2(t)\delta_{ij}dx^i dx^j, \tag{2.5}$$

where $a(t)$ is a time-dependent scale factor. On this background, the Friedmann and scalar field equations of motion are

$$3(M^2_{\rm Pl}+\xi\phi^2)H^2 = \frac{1}{2}\dot{\phi}^2 + V(\phi) - 6(\xi\phi + 4H^2\mu_{,\phi})H\dot{\phi}, \tag{2.6}$$

$$\ddot{\phi} + 3H\dot{\phi} + V_{,\phi} - 6\xi\phi(2H^2+\dot{H}) - 24\mu_{,\phi}H^2(H^2+\dot{H}) = 0, \tag{2.7}$$

where a dot represents a derivative with respect to t, $H=\dot{a}/a$ is the Hubble expansion rate, and we use the notations $\mu_{,\phi} = d\mu/d\phi$ and $V_{,\phi} = dV/d\phi$. Taking the time derivative of Eq. (2.6) and using Eq. (2.7), we obtain the closed-form differential equations

$$\begin{aligned}\dot{H} = \frac{1}{2\mathcal{D}}[&8\mu_{,\phi}H^2(V_{,\phi} - 18\xi\phi H^2 - 24\mu_{,\phi}H^4) \\ &+ 2\xi\phi(V_{,\phi} - 12\xi\phi H^2) - \dot{\phi}^2(2\xi+1+8\mu_{,\phi\phi}H^2) \\ &+ 8H\dot{\phi}(\xi\phi + 4\mu_{,\phi}H^2)],\end{aligned} \tag{2.8}$$

$$\ddot{\phi} + 3H\dot{\phi} + V_{\rm eff,\phi} = 0, \tag{2.9}$$

where

$$\begin{aligned}V_{\rm eff,\phi} \equiv \frac{1}{\mathcal{D}}[&(\xi\phi^2+M^2_{\rm Pl})(V_{,\phi} - 12\xi\phi H^2 - 24\mu_{,\phi}H^4) \\ &+ 3\dot{\phi}^2(2\xi+1+8\mu_{,\phi\phi}H^2)(\xi\phi+4\mu_{,\phi}H^2) \\ &+ 8H\dot{\phi}(\mu_{,\phi}V_{,\phi} - 3\xi^2\phi^2) \\ &- 288H^3\dot{\phi}\mu_{,\phi}(\xi\phi + 2H^2\mu_{,\phi})],\end{aligned} \tag{2.10}$$

$$\mathcal{D} \equiv (6\xi+1)\xi\phi^2 + M^2_{\rm Pl} + 8H\mu_{,\phi}(\dot{\phi} + 6\xi H\phi + 12H^3\mu_{,\phi}). \tag{2.11}$$

Notice that $V_{\rm eff}$ is an effective potential of the scalar field. Numerically, we solve Eqs. (2.8) and (2.9) for H and ϕ with the initial conditions of H, ϕ, and $\dot{\phi}$ consistent with the Hamiltonian constraint (2.6).

A. Linear perturbations and stability conditions

To study the evolution of cosmological perturbations during inflation, we consider a perturbed line element containing scalar perturbations α, ψ, ζ and tensor perturbations h_{ij} as

$$\begin{aligned}ds^2 = &-(1+2\alpha)dt^2 + 2\partial_i\psi dt dx^i \\ &+ a^2(t)[(1+2\zeta)\delta_{ij} + h_{ij}]dx^i dx^j.\end{aligned} \tag{2.12}$$

In full Horndeski theories including the action (2.1) as a special case, the linear perturbation equations of motion

[1] If we consider quantum corrections arising from the renormalization group running of the Standard Model, the Higgs self-coupling λ can be much smaller than 0.01, or even negative, at inflationary energy scales [110–114]. In this paper, we do not consider the runnings of coupling constants λ or ξ.

were already derived in the literature [105]. On using the Hamiltonian and momentum constraints to eliminate α and ψ and integrating the action (2.1) by parts, the second-order action of scalar perturbations is given by [104,105,118]

$$\mathcal{S}_s^{(2)} = \int \mathrm{d}t\mathrm{d}^3x\, a^3 Q_s \left[\dot{\zeta}^2 - \frac{c_s^2}{a^2}(\nabla\zeta)^2\right], \tag{2.13}$$

where

$$Q_s = 16\frac{\Sigma}{\Theta^2}Q_t^2 + 12Q_t, \quad c_s^2 = \frac{1}{Q_s}\left[\frac{16}{a}\frac{\mathrm{d}}{\mathrm{d}t}\left(\frac{a}{\Theta}Q_t^2\right) - 4c_t^2 Q_t\right], \tag{2.14}$$

with

$$Q_t = \frac{1}{4}\left(8H\mu_{,\phi}\dot{\phi} + M_{\rm Pl}^2 + \xi\phi^2\right),$$
$$c_t^2 = \frac{1}{4Q_t}\left(M_{\rm Pl}^2 + \xi\phi^2 + 8\mu_{,\phi\phi}\dot{\phi}^2 + 8\mu_{,\phi}\ddot{\phi}\right), \tag{2.15}$$

and

$$\Sigma = \frac{1}{2}\dot{\phi}^2 - 3H^2(M_{\rm Pl}^2 + \xi\phi^2) - 6\xi H\phi\dot{\phi} - 48H^3\mu_{,\phi}\dot{\phi},$$
$$\Theta = H(M_{\rm Pl}^2 + \xi\phi^2) + \xi\phi\dot{\phi} + 12H^2\mu_{,\phi}\dot{\phi}. \tag{2.16}$$

In the tensor sector, the reduced action is of the form

$$\mathcal{S}_t^{(2)} = \frac{1}{2}\int \mathrm{d}t\mathrm{d}^3x\, a^3 Q_t\left[\dot{h}_{ij}^2 - \frac{c_t^2}{a^2}(\nabla h_{ij})^2\right], \tag{2.17}$$

where Q_t and c_t^2 are as defined in Eq. (2.15). To avoid the ghost and Laplacian instabilities of scalar and tensor perturbations, we require the following conditions:

$$Q_s > 0, \qquad c_s^2 > 0, \qquad Q_t > 0, \qquad c_t^2 > 0. \tag{2.18}$$

On using the background in Eq. (2.6), we can express Q_t and Q_s in the forms

$$Q_t = \frac{1}{12H^2}\left[\frac{1}{2}\dot{\phi}^2 + V(\phi) - 6\xi H\phi\dot{\phi}\right],$$
$$Q_s = \frac{4\dot{\phi}^2}{\Theta^2}Q_t[2Q_t + 3(\xi\phi + 4H^2\mu_{,\phi})^2]. \tag{2.19}$$

Provided that ϕ decreases during inflation in the region $\phi > 0$, we have $-6\xi H\phi\dot{\phi} > 0$ for $\xi > 0$. In such cases, both Q_t and Q_s are positive, and hence the ghost instabilities are absent. In the absence of the scalar-GB coupling, both c_t^2 and c_s^2 are equivalent to 1. However, the deviations of c_t^2 and c_s^2 from 1 arise in theories with $\mu(\phi) \neq 0$, so we need to numerically compute c_t^2 and c_s^2 for a given coupling $\mu(\phi)$ to ensure the absence of Laplacian instabilities.

B. Higgs slow-roll inflation with $\mu(\phi) = 0$

We briefly revisit the background dynamics and perturbation spectra generated during Higgs slow-roll inflation for $\mu(\phi) = 0$. From Eqs. (2.6) and (2.9), we have

$$H^2 = \frac{1}{3(M_{\rm Pl}^2 + \xi\phi^2)}\left(\frac{1}{2}\dot{\phi}^2 + \frac{1}{4}\lambda\phi^4 - 6\xi H\phi\dot{\phi}\right), \tag{2.20}$$

$$\ddot{\phi} + 3H\dot{\phi} + \frac{(6\xi+1)\xi\phi\dot{\phi}^2}{(6\xi+1)\xi\phi^2 + M_{\rm Pl}^2} + \frac{\lambda\phi^3 M_{\rm Pl}^2}{(6\xi+1)\xi\phi^2 + M_{\rm Pl}^2} = 0. \tag{2.21}$$

Let us consider the large-coupling regime with $\xi \gg 1$ and $\xi\phi^2 \gg M_{\rm Pl}^2$. During slow-roll inflation, the dominant term in Eq. (2.20) is the potential $V(\phi) = \lambda\phi^4/4$, while the dominant contributions to Eq. (2.21) are the second and fourth terms. Then, Eqs. (2.20) and (2.21) approximately reduce to

$$H^2 \simeq \frac{\lambda\phi^2}{12\xi}, \qquad H\dot{\phi} \simeq -\frac{\lambda\phi M_{\rm Pl}^2}{18\xi^2}. \tag{2.22}$$

The field value ϕ_f at the end of inflation is determined by the condition $\epsilon_H \equiv -\dot{H}/H^2 = 1$. Using the two equations in Eq. (2.22), we have $\epsilon_H \simeq 2M_{\rm Pl}^2/(3\xi\phi^2)$, and hence $\phi_f = \sqrt{2/(3\xi)}M_{\rm Pl}$. The number of e-foldings counted backward from the end of inflation can be estimated as

$$N = \int_\phi^{\phi_f} \frac{H}{\dot{\phi}}\mathrm{d}\phi \simeq \frac{3\xi\phi^2}{4M_{\rm Pl}^2} - \frac{1}{2}, \tag{2.23}$$

where we exploit Eq. (2.22) in the second approximate equality. For $N \gg 1$, we obtain the simple relation $\phi^2 \simeq 4M_{\rm Pl}^2 N/(3\xi)$.

For perturbations deep inside the Hubble radius (with the wave number $k \gg aH$), they are initially in the Bunch-Davies vacuum state. On the inflationary background, ζ and h_{ij} approach constants after the sound horizon crossing. The power spectra of scalar and tensor perturbations generated during the quasi–de Sitter period are given, respectively, by [105]

$$\mathcal{P}_\zeta = \left.\frac{H^2}{8\pi^2 Q_s c_s^3}\right|_{c_s k = aH}, \qquad \mathcal{P}_h = \left.\frac{H^2}{2\pi^2 Q_t c_t^3}\right|_{c_t k = aH}. \tag{2.24}$$

In theories with $\mu(\phi) = 0$, we have $c_s^2 = 1 = c_t^2$, and hence both $\mathcal{P}_\zeta$ and $\mathcal{P}_h$ should be evaluated at $k = aH$.

Since $Q_s \simeq 3\xi\dot{\phi}^2/H^2$ and $Q_t \simeq \xi\phi^2/4$ in the regimes $\xi \gg 1$ and $\xi\phi^2 \gg M_{\rm Pl}^2$, the power spectra in Eq. (2.24) reduce to

$$\mathcal{P}_\zeta \simeq \frac{H^4}{24\pi^2\xi\dot{\phi}^2} \simeq \frac{\lambda\phi^4}{128\pi^2 M_{\rm Pl}^4} \simeq \frac{\lambda N^2}{72\pi^2\xi^2} \tag{2.25}$$

$$\mathcal{P}_h \simeq \frac{2H^2}{\pi^2\xi\phi^2} \simeq \frac{\lambda}{6\pi^2\xi^2}, \tag{2.26}$$

where we use the approximate background of Eq. (2.22). We note that the subscript $k = aH$ is omitted in Eqs. (2.25) and (2.26). Then, we obtain the scalar spectral index n_s and the tensor-to-scalar ratio r as

$$n_s - 1 = \left.\frac{\mathrm{d}\ln\mathcal{P}_\zeta}{\mathrm{d}\ln k}\right|_{k=aH} \simeq \frac{4\dot{\phi}}{H\phi} \simeq -\frac{8M_{\rm Pl}^2}{3\xi\phi^2} \simeq -\frac{2}{N}, \tag{2.27}$$

$$r = \frac{\mathcal{P}_h}{\mathcal{P}_\zeta} \simeq \frac{12}{N^2}. \tag{2.28}$$

Taking $N = 60$ for scales relevant to the observed CMB temperature anisotropies, we obtain $n_s = 0.9667$ and $r = 3.3 \times 10^{-3}$. These values are consistent with the bounds $n_s = 0.9661 \pm 0.0040$ (68% C.L.) and $r < 0.066$ (95% C.L.) constrained by the Planck 2018 data [84]. The Planck normalization $\mathcal{P}_\zeta = 2.1 \times 10^{-9}$ with $N = 60$ gives the constraint $\lambda/\xi^2 = 4.1 \times 10^{-10}$. If $\lambda = 0.1$, then $\xi = 1.6 \times 10^4$.

The above results are valid for slow-roll inflation with $\mu(\phi) = 0$. In the presence of the scalar-GB coupling, the background dynamics and perturbation spectra are subject to modifications. In subsequent sections, we will address this issue along with the problem of generating the source for PBHs.

III. EFFECTIVE POTENTIALS WITH PLATEAU AND BUMP

Let us proceed to the case in which the scalar-GB coupling $\mu(\phi)R^2_{\rm GB}$ is present. If $\mu(\phi)$ is a smooth function whose time variation is small during inflation, the inflaton field ϕ can slowly evolve along the potential. In such a case, the primordial power spectra of scalar and tensor perturbations are given by Eq. (2.24). Since Q_s is proportional to $\dot{\phi}^2$, a smaller inflaton velocity generally leads to a larger amplitude of $\mathcal{P}_\zeta$. In the context of slow-roll inflation, however, this enhancement of $\mathcal{P}_\zeta$ is limited by a small time variation of $\dot{\phi}$.

If the scalar-GB coupling generates a period in which the field velocity $\dot{\phi}$ temporally approaches 0, it is possible to realize the large enhancement of $\mathcal{P}_\zeta$ for scales smaller than those of the observed CMB temperature anisotropies. One possible choice of $\mu(\phi)$ is a dilatonic coupling of the form $\mu(\phi) = \mu_0 e^{-\lambda\phi}$ [100,119–124]. However, this type of continuously varying function affects not only the scalar perturbation on particular scales but also that on other scales including the CMB. Moreover, it can happen that the dominance of the scalar-GB coupling over the potential and nonminimal couplings leads to the violation of the stability conditions in Eq. (2.18).

Instead, we consider the steplike coupling given by [77,78,125]

$$\mu(\phi) = \mu_0 \tanh[\mu_1(\phi - \phi_c)], \tag{3.1}$$

where μ_0, μ_1, and ϕ_c are constants. Around the field value $\phi = \phi_c$, this coupling rapidly changes from the asymptotic constant $\mu(\phi) = -\mu_0$ (for $\phi \ll \phi_c$) to the other asymptotic constant $\mu(\phi) = +\mu_0$ (for $\phi \gg \phi_c$). Since the GB curvature invariant is a topological term, the scalar-GB coupling does not affect the cosmological dynamics in the two asymptotic regimes with constant $\mu(\phi)$. Provided that ϕ_c is in the range $\phi_f < \phi_c < \phi_{\rm CMB}$, where $\phi_{\rm CMB}$ is the field value about 60 e-foldings before the end of inflation (with the field value ϕ_f), it should be possible to enhance the scalar power spectrum for scales smaller than those of observed CMB temperature anisotropies. In Sec. IV, we will study whether the sufficient generation of seeds for PBHs is possible, while satisfying observational constraints on n_s and r on CMB scales.

Provided that the field kinetic term is sufficiently small during inflation, we can ignore the $\dot{\phi}$-dependent terms in Eq. (2.10). Then, the ϕ derivative of the effective potential $V_{\rm eff}$ is approximately given by

$$V_{{\rm eff},\phi} \simeq \frac{(\xi\phi^2 + M_{\rm Pl}^2)(V_{,\phi} - 12\xi\phi H^2 - 24\mu_{,\phi}H^4)}{(6\xi+1)\xi\phi^2 + M_{\rm Pl}^2 + 48H^2\mu_{,\phi}(\xi\phi + 2H^2\mu_{,\phi})}. \tag{3.2}$$

From Eq. (2.6), the Hubble parameter is approximately given by

$$H^2 \simeq \frac{V(\phi)}{3(M_{\rm Pl}^2 + \xi\phi^2)}. \tag{3.3}$$

Substituting Eq. (3.3) into Eq. (3.2) and integrating it with respect to ϕ, the effective potential $V_{\rm eff}$ can be numerically known as a function of ϕ.

In the following, we classify the effective potential into three classes: (i) plateau-type, (ii) bump-type, and (iii) intermediate-type. The Set 1, 2, and 3 model parameters shown in Table I are the typical examples of plateau, bump, and intermediate types, respectively. The nonminimal coupling constant is fixed to be $\xi = 5000$ in all cases.

Since PBHs are treated as the main component of DM in this paper, we consider the PBH mass range $10^{-16}M_\odot \lesssim M \lesssim 10^{-11}M_\odot$. This gives a constraint on the value of ϕ_c. The two constants μ_0 and μ_1 determine the types of $V_{\rm eff}(\phi)$ mentioned above. Instead of the parameter μ_0, we will use the combination

TABLE I. Three sets of model parameters. For dimensionful parameters, the units are given inside the squared parentheses.

	ξ	λ	$\phi_c[M_{\rm Pl}]$	$\mu_1[M_{\rm Pl}^{-1}]$	$\tilde{\mu}_0[10^8 M_{\rm Pl}^{-1}]$	rhs of Eq. (3.8) $[10^8 M_{\rm Pl}^{-1}]$
Set 1	5000	0.0244211	0.0380	1000	1.564709	1.556127
Set 2	5000	0.0110810	0.0760	5000	0.249909	0.176768
Set 3	5000	0.0152511	0.0600	1600	0.376125	0.366512

$$\tilde{\mu}_0 \equiv \frac{1}{4}\mu_0\mu_1\lambda, \tag{3.4}$$

which appears later in Eq. (3.8). The values of $\tilde{\mu}_0$ are chosen to be close to or not far away from the right-hand side (rhs) of Eq. (3.8); see the last two columns in Table I. The Higgs self-coupling λ is determined by the observed amplitude of primordial curvature perturbations on CMB scales. As we see in Table I, λ is of order 0.01 for the three sets of model parameters.

A. Plateau type

Thanks to the existence of the scalar-GB coupling, there is a stationary fixed point $\phi = \phi_*$ at which $V_{{\rm eff},\phi}$ vanishes [77]. From Eq. (3.2) combined with Eq. (3.3), we have the following relation:

$$V_{,\phi} - \frac{4\xi\phi V}{M_{\rm Pl}^2 + \xi\phi^2} - \frac{8\mu_{,\phi}V^2}{3(M_{\rm Pl}^2 + \xi\phi^2)^2}\bigg|_{\phi=\phi_*} = 0. \tag{3.5}$$

This is known as the USR regime, in which the scalar field equation (2.9) reduces to [44–46,49]

$$\ddot{\phi} + 3H\dot{\phi} \simeq 0 \qquad (\text{around}\,\phi = \phi_*). \tag{3.6}$$

The solution to this equation is given by

$$\dot{\phi} \propto a^{-3} \propto e^{-3n} \qquad (\text{around}\,\phi = \phi_*), \tag{3.7}$$

where $n = \ln a$ is the number of e-foldings counted forward. Hence, $\dot{\phi}$ rapidly decreases toward 0 in the USR regime.

Setting $\phi_* = \phi_c$ for the coupling in Eq. (3.1), the moment at which $V_{{\rm eff},\phi}$ vanishes coincides with the instant at the transition of $\mu(\phi)$. For the potential $V(\phi) = \lambda\phi^4/4$, the condition [Eq. (3.5)] translates to

$$\tilde{\mu}_0 = \frac{3M_{\rm Pl}^2(M_{\rm Pl}^2 + \xi\phi_c^2)}{2\phi_c^5}, \tag{3.8}$$

which gives a constraint between μ_0, μ_1, ϕ_c and λ, ξ. During the USR regime, the variation of the scalar field is of order $1/\mu_1$. Using Eqs. (2.22) and (3.7), we can estimate the order of $1/\mu_1$ as

$$\frac{1}{\mu_1} \simeq \int \frac{|\dot{\phi}|}{H}{\rm d}n \simeq \int_0^{\Delta N_c} \frac{2M_{\rm Pl}^2}{3\xi\phi_c} e^{-3n}{\rm d}n = \frac{2M_{\rm Pl}^2}{9\xi\phi_c}(1 - e^{-3\Delta N_c}), \tag{3.9}$$

where ΔN_c is the number of e-foldings acquired during the USR phase.

In the left panel of Fig. 1, we plot $V_{\rm eff}(\phi)$ in the vicinity of $\phi = \phi_c$ for the Set 1 model parameters given in Table I. In this case, $\tilde{\mu}_0$ is chosen to be close to the rhs of Eq. (3.8). There is a plateau of $V_{\rm eff}(\phi)$ in the region $|\phi - \phi_c| \lesssim 5 \times 10^{-4} M_{\rm Pl}$, where $\phi_c = 0.0380 M_{\rm Pl}$. In the left panel of Fig. 2, we show the evolution of ϕ versus the number of e-foldings for the parameter Set 1

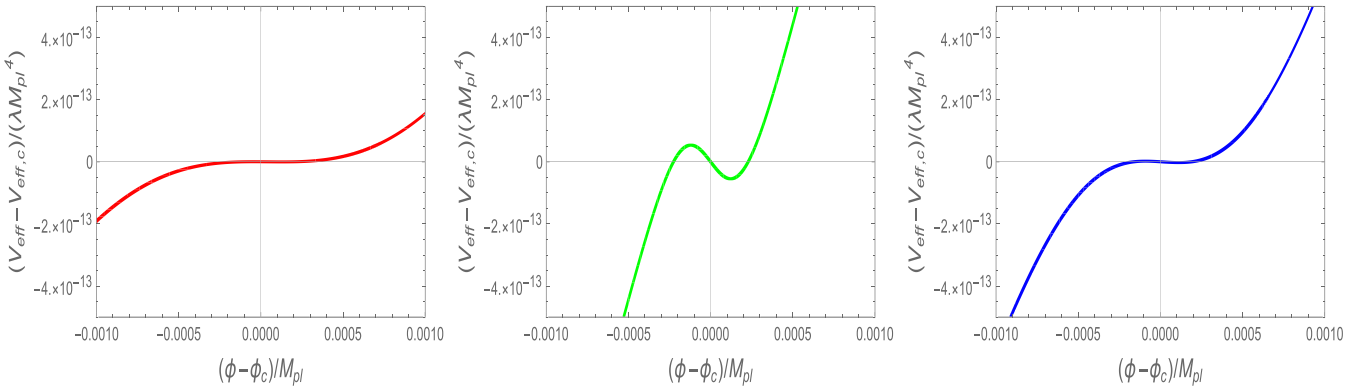

FIG. 1. Shapes of the effective potential $V_{\rm eff}(\phi)$ around $\phi = \phi_c$, where $V_{{\rm eff},c} = V_{\rm eff}(\phi_c)$. Each plot shows plateau-type (left), bump-type (middle), and intermediate-type (right).

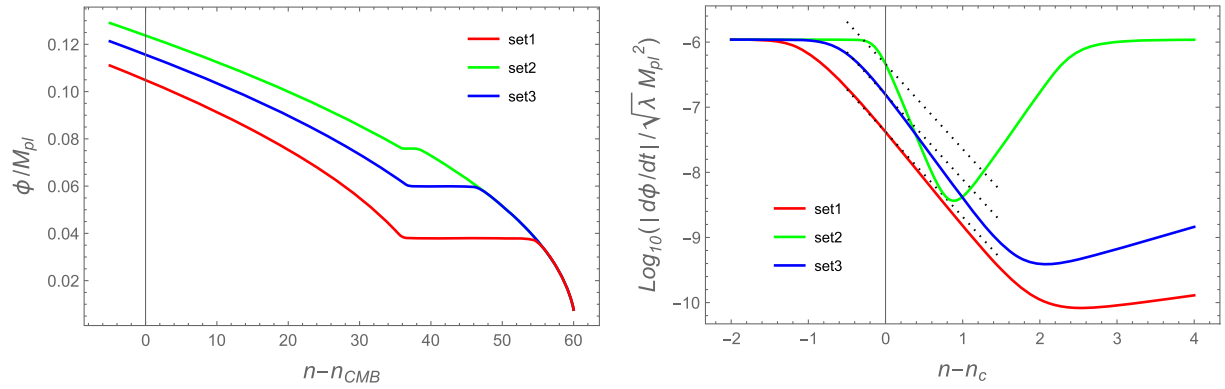

FIG. 2. Evolution of ϕ during inflation (left) and $|\dot{\phi}|$ around $\phi = \phi_c$ (right) for the three sets of parameters given in Table I. Here, n is the number of e-foldings counted forward toward the end of inflation, where $n_{\rm CMB}$ and n_c are the e-foldings corresponding to the field values $\phi_{\rm CMB}$ and ϕ_c, respectively. In the right panel, the dotted lines represent the evolution of $\dot{\phi}$ in the USR regime—i.e., $\dot{\phi} \propto e^{-3n}$.

as a red line. The field value ϕ_f at the end of inflation is numerically derived by the condition $\epsilon_H = 1$, which gives $\phi_f = 0.0077 M_{\rm Pl}$.

The initial field value for realizing the total number of e-foldings, $n - n_{\rm CMB} = 60$, by the end of inflation corresponds to $\phi_{\rm CMB} \simeq 0.105 M_{\rm Pl}$ (at which $n = n_{\rm CMB}$). In this case, the first slow-roll stage of inflation is followed by the USR period starting at $n - n_{\rm CMB} \simeq 36$. After the inflaton approaches the plateau of $V_{\rm eff}(\phi)$ around $\phi = \phi_c$, the field derivative rapidly decreases as $|\dot{\phi}| \propto e^{-3n}$; see the right panel of Fig. 2. For the model parameters of Set 1, the number of e-foldings acquired during the USR epoch is 18.6. Finally, the scalar field exits from the USR regime, after which $|\dot{\phi}|$ starts to increase.

As the plateau region of $V_{\rm eff}(\phi)$ gets wider, the number of e-foldings ΔN_c acquired during the USR phase tends to be larger. For ΔN_c exceeding the order 10, the CMB observables like n_s and r are subject to modifications in comparison to those derived for $\mu(\phi) = 0$. We will discuss this issue in Sec. IV.

B. Bump type

For the plateau-type effective potential, the scalar-GB coupling balances the contributions arising from the potential and nonminimal couplings in the scalar-field equation of motion. On the other hand, it should be possible that the scalar-GB term temporarily becomes larger than the contributions from other terms. This causes an instantaneous slowdown of the inflaton velocity in a manner different from the USR case discussed in Sec. III A. We call this class a "bump-type" model, in which the ϕ derivative of $V_{\rm eff}(\phi)$ has the following feature:

$$V_{{\rm eff},\phi}(\phi) = \begin{cases} > 0 & \text{for } \phi \gg \phi_c, \\ < 0 & \text{around } \phi = \phi_c, \\ > 0 & \text{for } \phi \ll \phi_c. \end{cases} \tag{3.10}$$

The parameter Set 2 in Table I gives rise to an effective potential of the bump type, which is illustrated in the middle panel of Fig. 1. In this case, $\tilde{\mu}_0$ exhibits some deviation from the value on the rhs of Eq. (3.8). The effective potential has a local maximum as well as a local minimum in the vicinity of $\phi = \phi_c$. We note that similar toy models have been studied in Refs. [57,58,73,75,80] in different contexts.

If $\tilde{\mu}_0$ is larger than the rhs of Eq. (3.8), the scalar-GB coupling dominates over the contributions from the potential and nonminimal couplings. However, the period of the dominance must be sufficiently short to end inflation properly. This requires that the parameter μ_1 is quite large. In the limit $\mu_1 \to \infty$, $\mu_{,\phi}$ and $\mu_{,\phi\phi}$ behave as

$$\lim_{\mu_1 \to \infty} \mu_{,\phi} = 2\mu_0 \delta(\phi - \phi_c), \tag{3.11}$$

$$\lim_{\mu_1 \to \infty} \mu_{,\phi\phi} = \mu_0 \mu_1 [\delta(\phi - (\phi_c - \epsilon)) - \delta(\phi - (\phi_c + \epsilon))], \tag{3.12}$$

where $\epsilon = \text{arctanh}(1/\sqrt{3})/\mu_1$. This type of steplike behavior for large μ_1 may induce Laplacian instabilities of cosmological perturbations, so we will address this issue in Sec. IV by computing the values of c_s^2 and c_t^2.

For the Set 2 model parameters corresponding to the bump-type effective potential, we plot the evolution of ϕ and $|\dot{\phi}|$ as a green line in Fig. 2. Unlike the plateau model, the field velocity decreases faster than $|\dot{\phi}| \propto e^{-3n}$ due to the existence of the region $V_{{\rm eff},\phi} < 0$ around $\phi = \phi_c$. When the field reaches a local maximum of $V_{\rm eff}(\phi)$, however, this period of the rapid decrease of $\dot{\phi}$ soon comes to end. After this short epoch, the scalar field quickly returns to the slow-roll evolution. As we see in the left panel of Fig. 2, the number of e-foldings ΔN_c acquired during the transient phase around $\phi = \phi_c$ is only a few, which is much smaller than ΔN_c in the USR case.

C. Intermediate type

Besides the two types of $V_{\rm eff}(\phi)$ discussed above, there is also an intermediate case between the plateau and bump types. In this case, the effective potential is not exactly flat in the vicinity of $\phi=\phi_c$, but it has a small peak and trough with a slight negative value of $V_{{\rm eff},\phi}$ around $\phi=\phi_c$. The Set 3 parameters in Table I give rise to such a shape of $V_{\rm eff}(\phi)$; see the right panel of Fig. 1.

As we plot with a blue line in Fig. 2, the field derivative initially decreases in proportion to $|\dot\phi|\propto e^{-3n}$, which is followed by a temporal period in which the decreasing rate of $|\dot\phi|$ becomes faster than $|\dot\phi|\propto e^{-3n}$. In this latter regime, the scalar field loses its velocity by climbing up the potential hill with $V_{{\rm eff},\phi}<0$. After the field reaches the local maximum of $V_{\rm eff}(\phi)$, $|\dot\phi|$ starts to grow toward the slow-roll regime. Since the effective potential has neither an exactly flat region nor a sharp bump, the number of e-foldings ΔN_c acquired around $\phi=\phi_c$ is between those of plateau and bump types. In Set 3 model parameters, we have $\Delta N_c\simeq 9.7$.

IV. GENERATION OF THE SEED FOR PBHs

In this section, we study how the power spectrum of curvature perturbations is enhanced by the presence of the scalar-GB coupling [Eq. (3.1)]. As we discussed in Sec. III, the inflaton effective potential $V_{\rm eff}(\phi)$ can be classified into three classes: (i) plateau-type, (ii) bump-type, and (iii) intermediate-type. Examples of the model parameters corresponding to each type of $V_{\rm eff}(\phi)$ are given in Table I as Sets 1, 2, and 3, respectively. In Sec. IV A, we first discuss whether each model satisfies the stability conditions in Eq. (2.18). In Sec. IV B, we compute the primordial scalar power spectra by paying particular attention to the enhancement of curvature perturbations around $\phi=\phi_c$. In Sec. IV C, we confront our models with the observed scalar spectral index and tensor-to-scalar ratio on CMB scales.

A. Stability conditions

Let us first study whether the stability conditions [Eq. (2.18)] can be satisfied during the whole stage of inflation. As we alluded to in Sec. II A, the no-ghost parameter Q_t in the tensor sector is positive for $\xi H\phi\dot\phi<0$. For the three sets of model parameters in Table I, the field derivative $\dot\phi$ is negative without reaching 0; see the right panel of Fig. 2. Then, we have $Q_t>0$, even during the transient epoch around $\phi=\phi_c$. From Eq. (2.19), the other no-ghost parameter Q_s is also positive for $Q_t>0$. Thus, the ghost instabilities are absent for both tensor and scalar perturbations, a property which is also confirmed numerically.

The scalar-GB coupling generally gives rise to tensor and scalar propagation speeds different from 1. In the left panel of Fig. 3, we show the evolution of c_t^2 versus the number of e-foldings, $n-n_{\rm CMB}$, for the three sets of model parameters in Table I. Just after the entry to the transient regime around $\phi=\phi_c$, c_t^2 exhibits the deviation from 1. During the USR stage realized for the Set 1 model parameters, the field velocity is significantly suppressed, and hence c_t^2 approaches 1. Just after the inflaton field exits from the USR regime, there is the temporal deviation of c_t^2 from 1. In the subsequent slow-roll regime, c_t^2 again goes back to 1. For the bump-type potential, which corresponds to the Set 2 model parameters, the time variation of c_t^2 occurs instantly in the vicinity of $\phi=\phi_c$. In all the cases shown in the left panel of Fig. 3, the deviation of c_t^2 from 1 is insignificant ($|c_t^2-1|\lesssim 0.04$), and hence the stability condition $c_t^2>0$ is always satisfied.

In the right panel of Fig. 3, we plot c_s^2 versus $n-n_{\rm CMB}$ for the same sets of model parameters as those used in the left. For scalar perturbations, the no-ghost quantity Q_s is proportional to $\dot\phi^2$. Since Q_s appears in the denominator of c_s^2 in Eq. (2.14), a smaller $\dot\phi^2$ does not imply a value of c_s^2 closer to 1. Indeed, during the transient regime around $\phi=\phi_c$, the scalar propagation speeds deviate from 1 in all three cases shown in Fig. 3. For Set 1, the minimum value

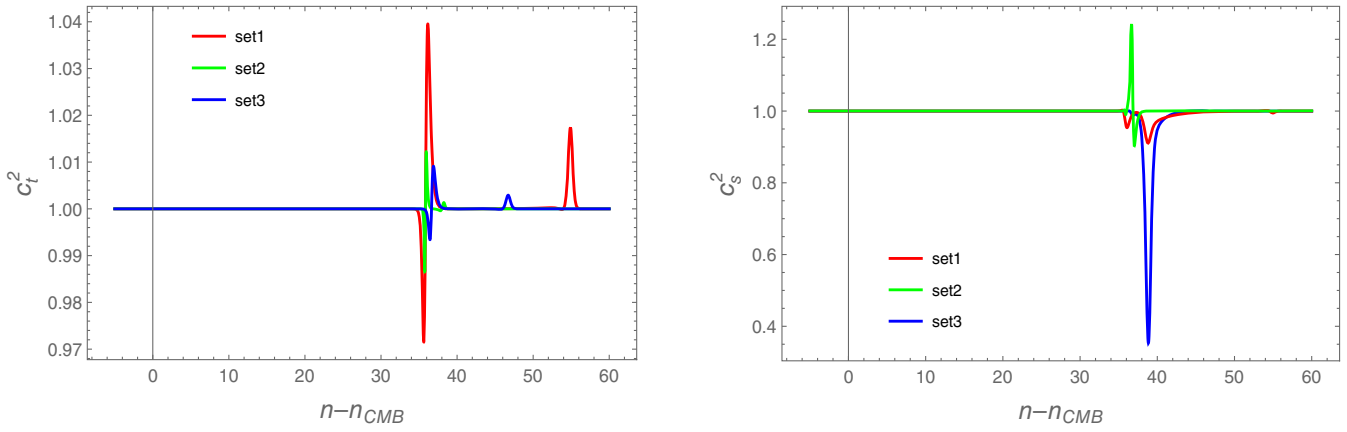

FIG. 3. Evolutions of c_t^2 (left) and c_s^2 (right) for the three sets of model parameters given in Table I.

of c_s^2 reached during the USR regime is about 0.91. The bump-type potential corresponds to the Set 2 model parameters, in which case c_s^2 temporally increases to the superluminal region and then quickly evolves to the minimum around $c_s^2 = 0.90$. For Set 3, c_s^2 decreases to the minimum around 0.35 and returns back to the value close to 1 in the slow-roll regime. Since the positivity of c_s^2 holds in all these cases, there are no Laplacian instabilities for scalar perturbations.

Depending on the model parameters, there are cases in which the scalar sound speed enters the region $c_s^2 < 0$. Since such models should be excluded by the Laplacian instability, we will focus on the case $c_s^2 > 0$ in subsequent sections.

B. Primordial scalar power spectrum

To study the evolution of curvature perturbations during inflation, we introduce the "sound horizon" time defined by

$$\tau_s = \int \mathrm{d}t \frac{c_s}{a}, \tag{4.1}$$

where $c_s > 0$. Then, the second-order action [Eq. (2.13)] of scalar perturbations reduces to

$$\mathcal{S}_s^{(2)} = \int \mathrm{d}\tau_s \mathrm{d}^3x\, a^2 Q_s c_s [\zeta'^2 - (\nabla\zeta)^2], \tag{4.2}$$

where a prime represents the derivative with respect to τ_s. We decompose the curvature perturbation into the Fourier modes ζ_k as

$$\zeta(\tau_s, \boldsymbol{x}) = \frac{1}{(2\pi)^3}\int \mathrm{d}^3k [\zeta_k(\tau_s, \boldsymbol{k}) a(\boldsymbol{k}) + \zeta_k^*(\tau_s, -\boldsymbol{k}) a^\dagger(-\boldsymbol{k})] e^{i\boldsymbol{k}\cdot\boldsymbol{x}}, \tag{4.3}$$

where $\boldsymbol{k}$ is a comoving wave number, and $a(\boldsymbol{k})$ and $a^\dagger(\boldsymbol{k})$ are annihilation and creation operators, respectively. Introducing the rescaled field

$$u_k = Z_s \zeta_k, \quad \text{with} \quad Z_s = a\sqrt{2Q_s c_s}, \tag{4.4}$$

we obtain the following differential equation:

$$u_k'' + \left(k^2 - \frac{Z_s''}{Z_s}\right) u_k = 0. \tag{4.5}$$

For the perturbations deep inside the sound horizon ($k^2 \gg a^2H^2/c_s^2$), Z_s''/Z_s is suppressed relative to k^2. For such modes, we choose a positive-frequency solution in a Bunch-Davies vacuum state—i.e.,

$$u_k = \frac{1}{\sqrt{2k}} e^{-ik\tau_s}, \tag{4.6}$$

as an initial condition. In practice, we set the initial time for each wave number that corresponds to six e-foldings before the sound-horizon crossing—i.e., at $k = e^6 aH/c_s$. Numerically, we integrate Eq. (4.5) by the end of inflation (characterized by the time $\tau_s = \tau_{sf}$) and compute the scalar power spectrum given by

$$\mathcal{P}_\zeta(k) = \frac{k^3}{2\pi^2} |\zeta_k(\tau_{sf}, \boldsymbol{k})|^2. \tag{4.7}$$

We evaluate $\mathcal{P}_\zeta(k)$ for three sets of model parameters given in Table I. At the 60 e-foldings before the end of inflation, the observed amplitude $\mathcal{P}_\zeta = 2.1 \times 10^{-9}$ on CMB scales is used to give a constraint among the model parameters. The two constants μ_0 and μ_1 in Table I are chosen to realize the sufficient enhancement of $\mathcal{P}_\zeta$ around $\phi = \phi_c$.

In Fig. 4, we show the primordial scalar power spectrum $\mathcal{P}_\zeta(k)$ for three sets of model parameters. In comparison to the value of $\mathcal{P}_\zeta$ on the CMB scale (characterized by the comoving wave number of order $k_{\mathrm{CMB}} = 10^{-3}$ Mpc), there is an enhancement of $\mathcal{P}_\zeta$ by a factor of 10^7. While the heights of peaks are similar between the three sets of parameters, the widths of $\mathcal{P}_\zeta$ are different from each other. The latter property is mostly attributed to the fact that the number of e-foldings ΔN_c acquired around $\phi = \phi_c$ are different between the plateau, bump, and intermediate types.

Let us try to understand how the enhancement of $\mathcal{P}_\zeta$ around $\phi = \phi_c$ occurs in detail. For the perturbations outside the sound horizon ($k^2 \ll a^2H^2/c_s^2$), Eq. (4.5) is approximately given by

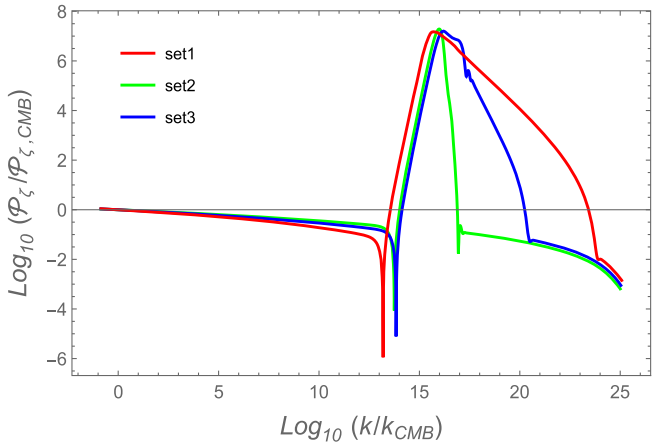

FIG. 4. The scalar power spectrum $\mathcal{P}_\zeta$ (normalized by its value on the CMB scale $\mathcal{P}_{\zeta,\mathrm{CMB}}$) versus the comoving wave number k (normalized by the wave number k_{CMB} on the CMB scale). Each plot corresponds to the three sets of model parameters presented in Table I.

$$u_k'' - \frac{Z_s''}{Z_s} u_k \simeq 0. \tag{4.8}$$

The solution to this equation can be generally expressed in the form

$$\zeta_k(\tau_s) = \frac{u_k(\tau_s)}{Z_s(\tau_s)} = A_k + B_k \int^{\tau_s} \frac{\mathrm{d}\tilde{\tau}_s}{Z_s^2(\tilde{\tau}_s)}, \tag{4.9}$$

where A_k and B_k are constants. On using the approximations $\Theta \simeq H\xi\phi^2$ and $Q_t \simeq V/(12H^2)$ in the regimes $\xi\phi^2 \gg M_{\rm Pl}^2$ and $\xi \gg 1$, the no-ghost parameter Q_s in Eq. (2.19) approximately reduces to

$$Q_s \simeq \frac{4(3\xi^2 + \lambda\mu_{,\phi}\phi)^2}{\lambda\xi^2\phi^2}\dot{\phi}^2, \tag{4.10}$$

which is positive. Since we are considering the scalar-field evolution with $\dot{\phi} < 0$, the quantity Z_s has the dependence

$$Z_s \simeq -2\sqrt{\frac{2c_s}{\lambda}}\frac{3\xi^2 + \lambda\mu_{,\phi}\phi}{\xi\phi} a\dot{\phi}. \tag{4.11}$$

During the slow-roll regime in which the contribution from the scalar-GB coupling is negligible, the field derivative $\dot{\phi}$ changes slowly with $c_s \simeq 1$. In the limit that $\dot{\phi}$ is constant, we have $Z_s \propto a$, and hence the last term of Eq. (4.9) decays in proportion to a^{-3} on the quasi–de Sitter background [where $a \simeq -(H\tau_s)^{-1}$]. Then, after the sound horizon crossing, ζ_k approaches a constant value A_k.

On the other hand, the field derivative exhibits a temporal rapid decrease during the transition around $\phi = \phi_c$. Since the scalar-field solution in the USR regime arising from the plateau-type effective potential is given by $\dot{\phi} \propto a^{-3}$, neglecting the time dependence of c_s leads to the approximate relation $Z_s \propto a^{-2}$. Then, the last term in Eq. (4.9) increases in proportion to a^3. This means that the decaying mode in the slow-roll regime is replaced by the rapidly growing mode in the USR regime. Since $\dot{\phi}$ also decreases rapidly for bump- and intermediate-type potentials, the curvature perturbation can be strongly enhanced around $\phi = \phi_c$ as well.

In the left panel of Fig. 5, we plot Z_s versus $n - n_c$ for three sets of model parameters in Table I. During the initial slow-roll regime, the evolution of Z_s is approximately given by $Z_s \propto a$ in all these three cases. For Set 1, which corresponds to the plateau-type potential, we find that Z_s decreases as $Z_s \propto a^{-2}$ in the vicinity of $\phi = \phi_c$ as expected. As we see in the right panel of Fig. 3, the deviation of c_s^2 from 1 is insignificant for Set 1 model parameters, and hence the evolution of Z_s is hardly affected by the variation of c_s^2.

The bump-type potential realized by Set 2 model parameters leads to a larger decreasing rate of Z_s around $\phi = \phi_c$ in comparison to the plateau type because of the stronger suppression of $\dot{\phi}$ (see the right panel of Fig. 2). For Set 2, the scalar sound speed temporally enters the region $c_s^2 > 1$ with a shorter transient period around $\phi = \phi_c$ in comparison to Set 1. For Set 3, which corresponds to the intermediate-type potential, the decreasing rate of Z_s is between those of the plateau and bump types. In all these cases, Z_s's begin to increase after reaching their minima, whose behavior is correlated with the evolution of $\dot{\phi}$ plotted in Fig. 2.

In the superhorizon regime, the enhancement of ζ_k depends on the integral of $1/Z_s^2(\tau_s)$ with respect to $\tau_s = \int \mathrm{d}t c_s/a$. On the other hand, we recall that we ignored the k^2 term in Eq. (4.5) relative to Z_s''/Z_s in the above argument. To understand which modes of ζ_k are subject to the amplification, we explicitly compute Z_s''/Z_s as

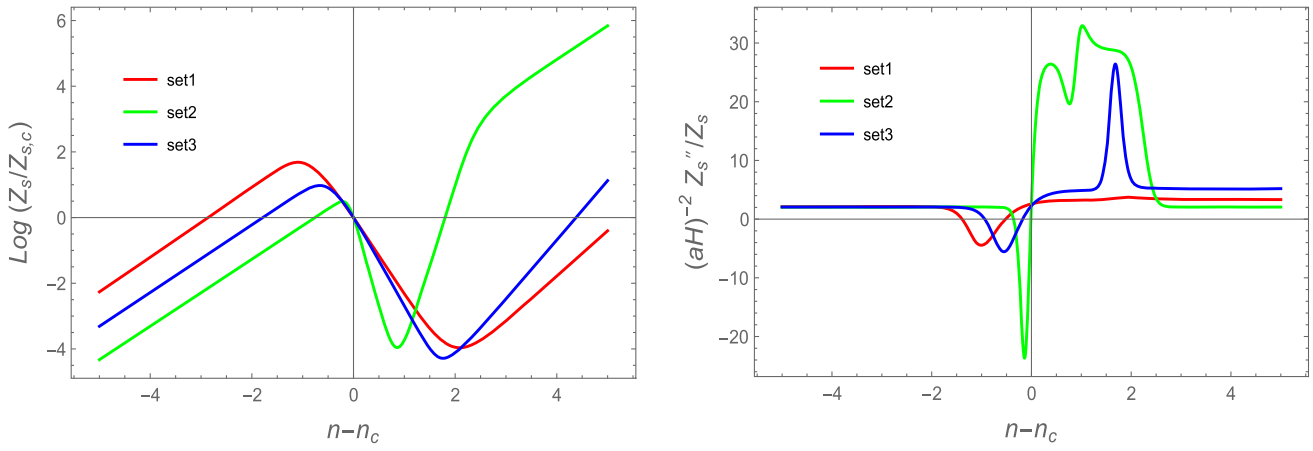

FIG. 5. Evolution of Z_s (left) and $(aH)^{-2}Z_s''/Z_s$ (right) around $n = n_c$ for three sets of model parameters given in Table I. Note that Z_s is normalized by the value $Z_{s,c}$ at $n = n_c$.

$$\frac{Z_s''}{Z_s} = \frac{(aH)^2}{c_s^2}\left[2 - \epsilon_H + \frac{3\epsilon_Q}{2} + \frac{\epsilon_c}{2} - \frac{1}{4}(\epsilon_c + \epsilon_Q)(2\epsilon_H - \epsilon_Q + \epsilon_c) + \frac{1}{2}(\epsilon_c\eta_c + \epsilon_Q\eta_Q)\right], \tag{4.12}$$

where

$$\epsilon_c \equiv \frac{\dot{c_s}}{Hc_s}, \qquad \epsilon_Q \equiv \frac{\dot{Q_s}}{HQ_s}, \qquad \eta_c \equiv \frac{\dot{\epsilon_c}}{H\epsilon_c}, \qquad \eta_Q \equiv \frac{\dot{\epsilon_Q}}{H\epsilon_Q}. \tag{4.13}$$

In the regime of slow-roll inflation, we have the approximate relation $Z_s''/Z_s \simeq 2(aH)^2$, and hence ζ_k soon approaches a constant after the Hubble radius crossing ($k \lesssim aH$). During the transient regime around $\phi = \phi_c$, the quantities defined in Eq. (4.13) can be larger than order 1. In the right panel of Fig. 5, we plot $\mathcal{Z} \equiv (aH)^{-2}Z_s''/Z_s$ versus $n - n_c$ for three sets of model parameters. For Set 1, $\mathcal{Z}$ starts to evolve from the value close to 2, temporally shows some decrease, and again increases to the value around 4. This means that, for the wave numbers in the range $k \lesssim 2aH$, there is the enhancement of ζ_k when the scalar field evolves along the plateau region of $V_{\rm eff}(\phi)$. For the perturbations which crossed the Hubble radius in the preceding slow-roll period, the last integral in Eq. (4.9) has already decayed sufficiently around the time at which ϕ approaches ϕ_c. Hence, the enhanced modes of ζ_k are those that crossed the Hubble radius during the transient epoch around $\phi = \phi_c$.

For Set 2, we observe in Fig. 5 that $\mathcal{Z}$ quickly reaches a value around 25 in the range $0 \lesssim n - n_c \lesssim 2$. This means that curvature perturbations up to the wave number $k \lesssim 5aH$, which include subhorizon modes, can be amplified. In comparison to Set 1, the shorter transient period around $\phi = \phi_c$ still limits the range of k for enhanced modes; see Fig. 4. Nevertheless, the height of the peak of $\mathcal{P}_\zeta(k)$ in Set 2 is similar to that in Set 1 thanks to the rapid increase of $\mathcal{Z}$. For Set 3, the enhanced scalar power spectrum spans in the ranges of k between those of Sets 1 and 2. In this case, the rapid decrease of c_s^2 seen in the right panel of Fig. 3 generates a sharp peak in $\mathcal{Z}$. This gives rise to a shape of $\mathcal{P}_\zeta(k)$ whose peak structure is different from those in other two cases. As we will see in Sec. V, the PBH abundance generated by these three sets of primordial power spectra can be sufficiently large to serve as almost all DM.

C. CMB constraints

The existence of the transient regime with strongly suppressed values of $\dot{\phi}$ modifies the spectra of scalar and tensor perturbations on scales relevant to the observed CMB temperature anisotropies. Besides Eq. (4.5), we also numerically solve the equation of tensor perturbations following from the second-order action [Eq. (2.17)]. We then compute the CMB observables like n_s, r, and $\mathcal{P}_\zeta$ around the $N_{\rm CMB} = 60$ e-foldings backward from the end of inflation.

As we see in Fig. 2, the inflaton field stays nearly constant in the region around $\phi = \phi_c$. In this transient regime, the acquired number of e-foldings ΔN_c is different depending on the model parameters. For larger ΔN_c, the field value $\phi_{\rm CMB}$ around the CMB scale tends to be smaller. Since ϕ stays nearly constant during the transient regime, we can simply replace the relation $\phi^2 \simeq 4M_{\rm Pl}^2 N/(3\xi)$ [which was derived for $\mu(\phi) = 0$ in the limit $N \gg 1$] with $\phi \to \phi_{\rm CMB}$ and $N \to N_{\rm CMB} - \Delta N_c$. Then, it follows that

$$\phi_{\rm CMB} \simeq 2\sqrt{\frac{N_{\rm CMB} - \Delta N_c}{3\xi}}M_{\rm Pl}. \tag{4.14}$$

In the USR case corresponding to the Set 1 model parameters in Fig. 2, we have $\Delta N_c = 18.6$ with $N_{\rm CMB} = 60$, and hence $\phi_{\rm CMB} \simeq 0.105 M_{\rm Pl}$ from Eq. (4.14). This shows good agreement with the numerical value of $\phi_{\rm CMB}$.

From Eqs. (2.25) and (2.26), the scalar power spectrum on CMB scales is known by the replacement $N \to N_{\rm CMB} - \Delta N_c$, while the tensor power spectrum is hardly subject to modifications by the scalar-GB coupling. Applying the change $N \to N_{\rm CMB} - \Delta N_c$ to Eqs. (2.25), (2.27), and (2.28), we obtain

$$\mathcal{P}_\zeta|_{\rm CMB} \simeq \frac{\lambda(N_{\rm CMB} - \Delta N_c)^2}{72\pi^2\xi^2}, \tag{4.15}$$

$$n_s - 1 \simeq -\frac{2}{N_{\rm CMB} - \Delta N_c}, \tag{4.16}$$

$$r \simeq \frac{12}{(N_{\rm CMB} - \Delta N_c)^2}. \tag{4.17}$$

For larger ΔN_c, these observables exhibit more significant deviations from those in standard Higgs inflation. The values of λ in Table I are chosen to match the amplitude $\mathcal{P}_\zeta|_{\rm CMB} = 2.1 \times 10^{-9}$ constrained by the Planck CMB data.

For the Set 1 model parameters in Table I, substituting $\Delta N_c = 20$ and $N_{\rm CMB} = 60$ into the analytic estimations of Eqs. (4.16) and (4.17) gives $n_s = 0.950$ and $r = 0.00750$. These are close to the numerically derived values presented in the first column of Table II. In Fig. 6, we show the 1σ and 2σ observational bounds constrained from Planck 2018 data combined with the data of B-mode polarizations available from the BICEP2/Keck field (BK14) and baryon acoustic oscillations (BAO) [84]. The theoretical values of n_s and r for Set 1 are outside the 2σ observational contour, so the plateau-type effective potential with $\Delta N_c = 18.6$ is disfavored from the data. Unless we choose an unusually

TABLE II. Numerical values of the scalar spectral index n_s and the tensor-to-scalar ratio r for three sets of model parameters given in Table I and Higgs inflation with $\mu(\phi) = 0$. The number of e-foldings on the CMB scale is fixed to be $N_{\rm CMB} = 60$.

	n_s	r
Set 1	0.951415	0.00757526
Set 2	0.965142	0.00347235
Set 3	0.960055	0.00476115
Higgs inflation	0.966527	0.00323724

large value of $N_{\rm CMB}$ exceeding 68, the model with $\Delta N_c \simeq 20$ does not enter the inside of the 2σ contour.

For Set 2, the number of e-foldings acquired around the bump region of $V_{\rm eff}(\phi)$ is as small as $\Delta N_c = 2.3$, so the CMB observables are similar to those in standard Higgs inflation; see the second and fourth columns in Table II. As we observe in Fig. 6, the model with Set 2 is inside the 1σ observational contour. For Set 3, we numerically obtain the values of n_s and r given in the third column of Table II, with $\Delta N_c = 9.7$. In this case, the model is between 1σ and 2σ observational contours in the (n_s, r) plane. For $N_{\rm CMB} = 60$, the number of e-foldings acquired around $\phi = \phi_c$ should be within the ranges

$$0 \le \Delta N_c < 7.6 \qquad (1\sigma), \tag{4.18}$$

$$7.6 \le \Delta N_c < 12.5 \qquad (2\sigma), \tag{4.19}$$

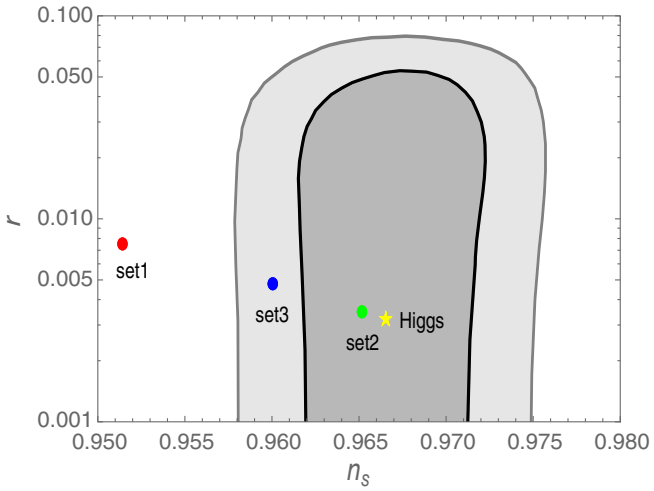

FIG. 6. Dark gray and light gray areas represent the 1σ and 2σ observational regions, respectively, constrained by the joint data analysis of Planck 2018 + BK14 + BAO at $k = 0.002$ Mpc^{-1}. The red, green, and blue points correspond to the theoretical predictions of n_s and r for the model parameters of Sets 1, 2, and 3, respectively, while the yellow star represents that of Higgs inflation. The number of e-foldings on the CMB scale is fixed to be $N_{\rm CMB} = 60$.

for consistency with observations of n_s and r at the 1σ and 2σ confidence levels, respectively. Thus, the bump-type model with $\Delta N_c =$ a few is favored over the plateau-type model with $\Delta N_c > 12.5$ from the viewpoint of CMB constraints.

Upon using the Planck-normalized value $\mathcal{P}_{\zeta|\rm CMB} = 2.1 \times 10^{-9}$ in Eq. (4.15) together with Eq. (4.16), we obtain the following relations:

$$\frac{\lambda}{\xi^2} \simeq \frac{1.49 \times 10^{-6}}{(N_{\rm CMB} - \Delta N_c)^2} \simeq 3.73 \times 10^{-7}(n_s - 1)^2. \tag{4.20}$$

Fixing $N_{\rm CMB}$ to be 60, the scalar spectral index is in the range $n_s = 1 - 2/(60 - \Delta N_c) \le 0.9667$ for $\Delta N_c \ge 0$. This means that, from Eq. (4.20), the ratio λ/ξ^2 is in the range $\lambda/\xi^2 \ge 4.1 \times 10^{-10}$. As ΔN_c increases, λ/ξ^2 gets larger. The 1σ and 2σ confidence regions of ΔN_c, which are given by Eqs. (4.18) and (4.19) respectively, translate to

$$4.1 \times 10^{-10} \le \frac{\lambda}{\xi^2} < 5.4 \times 10^{-10} \qquad (1\sigma), \tag{4.21}$$

$$5.4 \times 10^{-10} \le \frac{\lambda}{\xi^2} < 6.6 \times 10^{-10} \qquad (2\sigma), \tag{4.22}$$

In Fig. 7, these parameter spaces are plotted as yellow (1σ) and blue (2σ) regions in the (λ, ξ) plane. The red region is outside the 2σ observational contour. The allowed parameter spaces shown in Fig. 7 will be useful to put further constraints on the values of λ and ξ from future collider experiments.

V. PBH ABUNDANCE

After inflation, the perturbations reenter the Hubble radius, whose epoch depends on the comoving wave number k. In Sec. IV, we showed that the presence of the scalar-GB coupling can lead to the sufficient amplification of curvature perturbations during inflation for particular wavelengths smaller than the CMB scale ($k^{-1} \simeq 10^3$ Mpc). Such overdense regions can collapse to form PBHs after the horizon reentry.

The horizon mass associated with the Hubble distance H^{-1} is given by $M_H = 4\pi M_{\rm Pl}^2 H^{-1}$. The mass of PBHs at its formation time $t_{\rm form}$ can be expressed as [126]

$$M = \gamma M_H = 4\pi\gamma M_{\rm Pl}^2 H(t_{\rm form})^{-1}, \tag{5.1}$$

where γ is the ratio of how much of the inner region of the Hubble radius collapses into PBHs. We will consider the case in which the formation of PBHs occurs during the radiation-dominated epoch. The Hubble parameter at $t = t_{\rm form}$ is related to today's Hubble constant H_0 as [77]

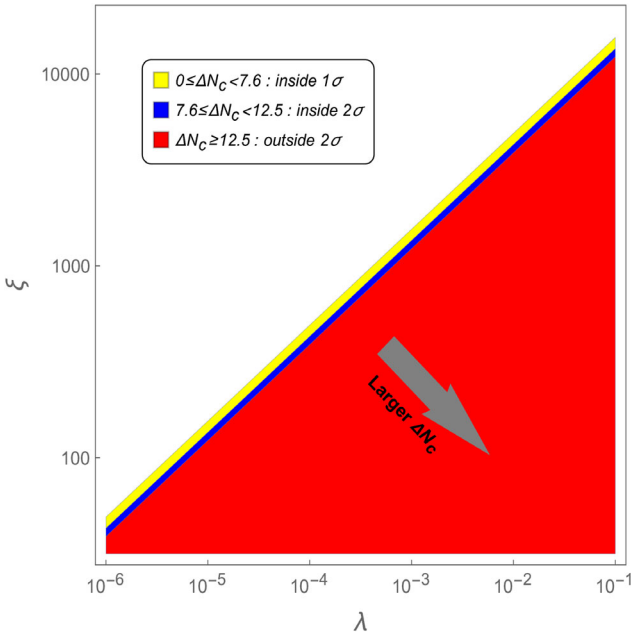

FIG. 7. 1σ (yellow) and 2σ (blue) confidence level parameter spaces in the (λ, ξ) plane constrained from the observed CMB temperature anisotropies with $\mathcal{P}_\zeta = 2.1 \times 10^{-9}$ and $N_{\rm CMB} = 60$. The 1σ and 2σ regions correspond to ΔN_c in the ranges given in Eqs. (4.18) and (4.19), respectively. The red region is outside the 2σ observational contour.

$$\frac{H(t_{\rm form})}{H_0} = \sqrt{\Omega_{r0}}\left[\frac{a_0}{a(t_{\rm form})}\right]^2\left[\frac{g_{*0}}{g_*(t_{\rm form})}\right]^{1/6}, \tag{5.2}$$

where the subscript "0" represents today's values and g_* is the relativistic degrees of freedom. The wave number at horizon reentry corresponds to $k = a(t_{\rm form})H(t_{\rm form})$, whose relation can be used to eliminate $a(t_{\rm form})$ in Eq. (5.2). Solving Eq. (5.2) for $H(t_{\rm form})$ and substituting it into Eq. (5.1), it follows that

$$M(k) = 10^{-13} M_\odot \left(\frac{\gamma}{0.2}\right)\left[\frac{g_*(t_{\rm form})}{106.75}\right]^{-1/6} \times \left(\frac{k}{4.9 \times 10^{12}\ {\rm Mpc}^{-1}}\right)^{-2}, \tag{5.3}$$

where we use the values $g_{*0} = 3.36$, $\Omega_{r0} = 9 \times 10^{-5}$, and $H_0 = 10^{-42}$ GeV.

The abundance of PBHs can be estimated by using the Press-Schechter theory. Assuming a Gaussian distribution for the coarse-grained density fluctuation δ_g, the probability that δ_g is higher than a certain threshold value δ_c at $t = t_{\rm form}$ is given by [126–129]

$$\beta(M(k)) = \int_{\delta_c}^{\infty} \frac{1}{\sqrt{2\pi\sigma^2(k)}} \exp\left[-\frac{\delta_g^2}{2\sigma^2(k)}\right] {\rm d}\delta_g, \tag{5.4}$$

where

$$\delta_g(\boldsymbol{x}, R) \equiv \int W(|\boldsymbol{x} - \boldsymbol{y}|, R)\delta(\boldsymbol{y}) {\rm d}^3 y. \tag{5.5}$$

The window function $W(|\boldsymbol{x} - \boldsymbol{y}|, R)$ determines how the density contrast $\delta = (\rho - \bar{\rho})/\bar{\rho}$ around $\boldsymbol{x}$ is coarse-grained, where ρ is the density and $\bar{\rho}$ is its background part. We choose the Gaussian window function of the form

$$W(|\boldsymbol{x} - \boldsymbol{y}|, R) = \frac{1}{(2\pi)^{3/2} R^3} \exp\left(-\frac{|\boldsymbol{x} - \boldsymbol{y}|^2}{2R^2}\right), \tag{5.6}$$

where the distance R is taken to be k^{-1}. Then, the variance of δ_g is given by

$$\sigma^2(k) = \frac{16}{81} \int \exp\left[-\left(\frac{p}{k}\right)^2\right]\left(\frac{p}{k}\right)^4 \mathcal{P}_\zeta(p) {\rm d} \ln\, p. \tag{5.7}$$

Since the PBH density decreases as $\rho_{\rm PBH} \propto a^{-3}$ after its formation, today's PBH density can be estimated as

$$\rho_{\rm PBH,0} = \rho_{\rm PBH}(t_{\rm form})\left[\frac{a_0}{a(t_{\rm form})}\right]^{-3} = \gamma\beta\rho_r(t_{\rm form})\left[\frac{a_0}{a(t_{\rm form})}\right]^{-3}. \tag{5.8}$$

Since $\rho_r(t_{\rm form})$ is related to $H(t_{\rm form})$ as $\rho_r(t_{\rm form}) = 3M_{\rm Pl}^2 H(t_{\rm form})^2$, today's density parameter of PBHs corresponding to Eq. (5.8) is

$$\Omega_{\rm PBH,0} = \frac{\rho_{\rm PBH,0}}{3M_{\rm Pl}^2 H_0^2} = \gamma\beta \frac{H(t_{\rm form})^2}{H_0^2}\left[\frac{a(t_{\rm form})}{a_0}\right]^3, \tag{5.9}$$

with total PBH density parameter $\int \Omega_{\rm PBH,0} {\rm d} \ln M$. Then, we obtain the ratio of the PBH abundance in a mass range $[M, M + {\rm d} \ln M]$ to the entire density of cold DM (today's density parameter $\Omega_{\rm CDM,0}$) as

$$f(M) = \frac{\Omega_{\rm PBH,0}}{\Omega_{\rm CDM,0}} \simeq \left[\frac{\beta(M)}{1.04 \times 10^{-14}}\right]\left(\frac{\gamma}{0.2}\right)^{3/2}\left[\frac{g_*(t_{\rm form})}{106.75}\right]^{-1/4} \times \left(\frac{\Omega_{\rm CDM,0}h^2}{0.12}\right)^{-1}\left(\frac{M}{10^{-13}M_\odot}\right)^{-1/2}, \tag{5.10}$$

where $H_0 = 100\ h\,{\rm km\,sec^{-1}\,Mpc^{-1}}$.

In the following, we use the values $\gamma = 0.2$ [130], $g_*(t_{\rm form}) = 106.75$, $\Omega_{\rm CDM,0}h^2 = 0.12$, and $\delta_c = 0.4$ for the computations of M and $f(M)$. With a given wave number k at horizon reentry, the PBH mass $M(k)$ is known from Eq. (5.3). The variance (5.7) is affected by the primordial spectrum $\mathcal{P}_\zeta(k)$ enhanced at some particular scales during inflation. This modifies the PBH mass function $f(M)$ through the change of $\beta(M(k))$ in Eq. (5.4).

In Fig. 8, we plot $f(M)$ versus M for the three sets of model parameters presented in Table I. In these

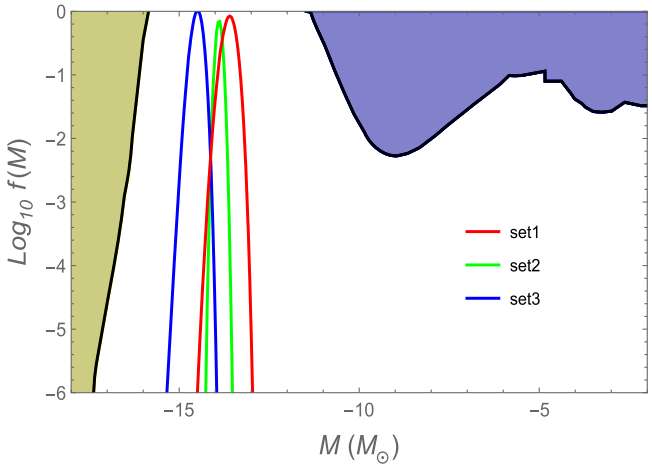

FIG. 8. The ratio of PBH abundances $f(M)$ relative to all the cold DM density as a function of the PBH mass M (in the unit of solar mass $M_\odot$) for the three sets of model parameters presented in Table I. The colored areas correspond to excluded regions from the evaporation of black holes (dark yellow) and observational constraints from the microlensing (dark blue). These observational constraints are taken from Refs. [9,131]. The list of references used to derive these constraints can be found in [132].

three cases, the mass functions $f(M)$ span the range $10^{-16}M_\odot \lesssim M \lesssim 10^{-13}M_\odot$. As we observe in Fig. 4, the wave number k corresponding to the peak positions of $\mathcal{P}_\zeta(k)$ is smallest for Set 1, while it is largest for Set 3. From Eq. (5.3), the PBH mass M decreases for larger k. Then, the mass M corresponding to the peaks of $f(M)$ is smallest for Set 3, while it is largest for Set 1. The maximum values of $f(M)$ are found to be 0.85, 0.71, and 1 for Sets 1, 2, and 3, respectively, so PBHs are the source for practically all cold DM in these three cases.

In Fig. 8, we also show the regions excluded by the black hole evaporation and by microlensing observations. The models with Sets 1, 2, 3 are also consistent with such constraints. While we have considered the PBH mass range $10^{-16}M_\odot \lesssim M \lesssim 10^{-13}M_\odot$, it is also possible to produce PBHs with the mass $M > 10^{-13}M_\odot$ by choosing different sets of model parameters. The heights of peaks of $f(M)$ can be also lower than the order 0.1 to be consistent with the microlensing data. Thus, our model allows versatile possibilities for generating PBHs in broad mass ranges.

Finally, we explicitly derive a relation between M and the critical field value ϕ_c. This is useful for estimating the mass of PBH and determining the model parameters. After the transient regime, the inflationary dynamics rapidly approaches the slow-roll solution, so we can exploit Eq. (2.23) as a good approximation. Then, we obtain

$$\frac{3\xi\phi_c^2}{4M_{\rm Pl}^2} \simeq N_{\rm CMB} - \ln\frac{a(t_{\rm PBH})}{a(t_{\rm CMB})} - \Delta N_c, \tag{5.11}$$

where $t_{\rm CMB}$ and $t_{\rm PBH}$ represent the moments at which the CMB and PBH scales leave the Hubble horizon, respectively. From Eq. (5.3), we can estimate $a(t_{\rm PBH})/a(t_{\rm CMB})$ as

$$\begin{aligned}\frac{a(t_{\rm PBH})}{a(t_{\rm CMB})} \simeq \frac{k}{k_{\rm CMB}} &\simeq \left[\frac{10^{-13}M_\odot}{M(k)}\right]^{1/2}\left(\frac{\gamma}{0.2}\right)^{1/2}\left[\frac{g_*(t_{\rm form})}{106.75}\right]^{-1/12} \\ &\times\left(\frac{4.9\times10^{12}\ {\rm Mpc}^{-1}}{k_{\rm CMB}}\right) \\ &\simeq \left[\frac{6\times10^{17}M_\odot}{M(k)}\right]^{1/2},\end{aligned} \tag{5.12}$$

where we use the values $\gamma = 0.2$, $g_*(t_{\rm form}) = 106.75$, and $k_{\rm CMB} = 0.002\ {\rm Mpc}^{-1}$ in the last equality. Substituting Eq. (5.12) into Eq. (5.11), it follows that

$$\phi_c \simeq M_{\rm Pl}\sqrt{\frac{4}{3\xi}\left\{N_{\rm CMB} - \Delta N_c + \frac{1}{2}\ln\left[\frac{M(k)}{6\times10^{17}M_\odot}\right]\right\}}. \tag{5.13}$$

In the USR case corresponding to Set 1 model parameters, for example, we have $\Delta N_c = 18.6$ and $M \simeq 4\times10^{-14}M_\odot$, and hence $\phi_c \simeq 0.0383M_{\rm Pl}$ from Eq. (5.13). This is in good agreement with the exact value of ϕ_c—i.e., $\phi_c = 0.0380M_{\rm Pl}$. For the PBH mass range $10^{-16}M_\odot \lesssim M \lesssim 10^{-11}M_\odot$ in which PBHs can be the source for all DM, the corresponding region of ϕ_c is given by

$$M_{\rm Pl}\sqrt{\frac{4}{3\xi}(21-\Delta N_c)} \lesssim \phi_c \lesssim M_{\rm Pl}\sqrt{\frac{4}{3\xi}(27-\Delta N_c)}. \tag{5.14}$$

We recall that, for the plateau-type potential, $\tilde{\mu}_0$ and μ_1 are related to ϕ_c according to Eqs. (3.8) and (3.9), respectively. By using these relations with Eq. (5.13), the orders of parameters $\tilde{\mu}_0$ and μ_1 are known for given values of $M(k)$ and ΔN_c. We caution that the relations (3.8) and (3.9) lose their accuracy for the bump-type potential, but they are still useful to estimate the orders of $\tilde{\mu}_0$ and μ_1. To know the precise values of $\tilde{\mu}_0$ and μ_1 with which curvature perturbations are sufficiently enhanced for scales relevant to PBHs, the numerical analysis is required as we performed in Sec. IV. Basically, $\tilde{\mu}_0$ and μ_1 determine the height of enhancement of ζ and the length of the transient period, respectively.

VI. CONCLUSIONS

We studied a mechanism for producing the seed of PBHs in Higgs inflation in the presence of a scalar-GB coupling. This provides a minimal scenario of inflation within the framework of the Standard Model of particle physics, while allowing for compatibility with observed CMB temperature anisotropies. In comparison to original Higgs inflation, however, the scalar-GB coupling can modify theoretical

predictions of the scalar spectral index and tensor-to-scalar ratio on CMB scales. We explored the possibility for enhancing curvature perturbations at some particular scales to generate the seed for PBHs, while the model is still compatible with the CMB observations.

The enhancement of curvature perturbations during inflation is possible when the inflaton velocity $\dot{\phi}$ rapidly decreases toward 0 during some transient epoch. If there is a period in which the scalar-GB coupling $\mu(\phi)$ quickly changes, it is possible to generate particular shapes in the inflaton effective potential $V_{\rm eff}(\phi)$. For this purpose, we considered a coupling function of the form $\mu(\phi) = \mu_0 \tanh[\mu_1(\phi - \phi_c)]$, where ϕ_c is the field value at transition. Since $\mu(\phi)$ approaches constants in two asymptotic regimes $\phi \ll \phi_c$ and $\phi \gg \phi_c$, the scalar-GB coupling affects the dynamics of background and perturbations only in the vicinity of $\phi = \phi_c$. Depending on the model parameters, the effective potential can be classified into three classes: (i) plateau-type, (ii) bump-type, and (iii) intermediate-type.

A typical example of the plateau type is the Set 1 model parameters given in Table I, in which case the scalar-GB coupling almost balances the potential and nonminimal coupling terms around $\phi = \phi_c$. For this type, the effective potential has a nearly flat region, as seen in the left panel of Fig. 1. During the USR regime, the field derivative decreases as $\dot{\phi} \propto a^{-3}$. As we observe in the left panel of Fig. 2 for Set 1, the number of e-foldings ΔN_c acquired around $\phi = \phi_c$ is as large as 20. The Set 2 model parameters in Table I give rise to a bump-type potential illustrated in the middle panel of Fig. 1. In this case, the existence of an explicit peak in $V_{\rm eff}(\phi)$ leads to the approach of $\dot{\phi}$ toward 0 even faster than the USR case. For Set 2, the number of e-foldings ΔN_c acquired around $\phi = \phi_c$ is as small as a few. The Set 3 model parameters in Table I correspond to the intermediate-type potential plotted in the right panel of Fig. 1. For this type, both the decreasing rate of $\dot{\phi}$ and ΔN_c are between those of the plateau and bump types.

The evolution of scalar perturbations during inflation crucially depends on the quantity Z_s defined in Eq. (4.4). After the sound horizon crossing, the solution to the Fourier-transformed curvature perturbation ζ_k is expressed in the form (4.9). In all three types of $V_{\rm eff}(\phi)$ mentioned above, Z_s rapidly decreases in the vicinity of $\phi = \phi_c$. Since the last integral in Eq. (4.9) becomes a rapidly growing mode during the transient regime, there is the strong enhancement of ζ_k for the modes exiting the sound horizon around $\phi = \phi_c$. For an effective potential closer to the bump type, the quantity Z_s''/Z_s, which appears in the equation of motion for $u_k = Z_s\zeta_k$, can exceed the order of $10(aH)^2$ during the rapid transition. Then, the bump-type potential also leads to the amplification of some subhorizon modes. Still, the shapes of primordial scalar power spectra $\mathcal{P}_\zeta(k)$ mostly depend on the number of e-foldings ΔN_c, in such a way that the peak tends to be sharper for smaller ΔN_c.

The primordial power spectra $\mathcal{P}_\zeta(k)$ plotted in Fig. 4 correspond to those of the Set 1, 2, 3 model parameters. In all these cases, the peak values of $\mathcal{P}_\zeta(k)$ are about 10^7 times as large as the amplitude of $\mathcal{P}_\zeta(k)$ on CMB scales. With these model parameters, all the stability conditions given in Eq. (2.18) are consistently satisfied, and hence there are neither ghost nor Laplacian instabilities. We note that the inflaton-GB coupling gives rise to a scalar propagation speed different from 1, whose property also affects the shapes of $\mathcal{P}_\zeta(k)$.

The existence of the transient epoch around $\phi = \phi_c$ modifies the scalar power spectrum and tensor-to-scalar ratio on CMB scales. In standard Higgs inflation, the expressions of $\mathcal{P}_\zeta$, n_s, and r are given, respectively, by Eqs. (2.25), (2.27), and (2.28), where N is the number of e-foldings counted backward from the end of inflation. In the presence of the scalar-GB coupling, these observables are subject to the modification $N \to N_{\rm CMB} - \Delta N_c$, where $N_{\rm CMB}$ corresponds to the number of e-foldings on CMB scales. This means that, for smaller ΔN_c, the models can exhibit better compatibility with the observational bounds on n_s and r. As we see in Fig. 6, the bump type with $\Delta N_c = 2.3$ (Set 2) is well inside the 1σ observational contour constrained from CMB and other data, while the plateau type with $\Delta N_c = 18.6$ (Set 1) is outside the 2σ contour. The intermediate-type model with $\Delta N_c = 9.7$ (Set 3) is between 1σ and 2σ contours. These results show that the bump type is generally favored over the plateau type from the CMB constraints.

In Fig. 8, we plot the PBH fraction function $f(M)$ versus the mass M for three sets of model parameters in Table I. In all these cases, we have $f(M) \simeq 1$ in the mass range $10^{-16}M_\odot \lesssim M \lesssim 10^{-13}M_\odot$. Thus, the GB-corrected Higgs inflation allows the possibility for generating the amount of PBHs serving as almost all DM, while being compatible with the observed temperature anisotropies on CMB scales especially for the bump-type effective potential. We note that, in our model, it is also possible to generate PBHs in the larger mass range $M > 10^{-13}M_\odot$ with the fraction $f(M) \lesssim 0.1$.

The enhanced primordial curvature perturbations on particular scales may induce gravitational waves at nonlinear order, which affects the spectrum of the gravitational wave background [133] (see also Ref. [134]). In addition, while a Gaussian distribution was used for the coarse-grained density fluctuation in this paper, it was reported that the distribution function of curvature fluctuations may have a peculiar shape deviating from the Gaussian [57,58,75,80,135–142]. Recently, it was shown that the PBH scenario in single-field inflation with an USR regime can induce large one-loop corrections to the scalar power spectrum on CMB scales [143,144]. Since the analysis is limited to a canonical scalar field with a plateau-type potential, the results of Ref. [143] are not applied to our model, in which the enhancement of curvature

perturbations occurs by the presence of the inflaton-GB coupling. However, it is worth computing one-loop corrections to $\mathcal{P}_\zeta$ in our model, especially for the bump-type effective potential. We leave these interesting issues for future works.

ACKNOWLEDGMENTS

We thank Tomohiro Fujita for useful discussions and comments. We also thank Bradley Kavanagh for giving us permission to use observational constraints given in Fig. 8. S. T. is supported by the Grant-in-Aid for Scientific Research Fund of the JSPS No. 19K03854 and No. 22K03642.

APPENDIX: CORRESPONDENCE WITH HORNDESKI THEORY

The inflationary model studied in this paper belongs to a subclass of Horndeski theory given by the action [105,115–117]

$$\mathcal{S} = \int \mathrm{d}^4x\sqrt{-g}\mathcal{L}_H, \tag{A1}$$

where

$$\mathcal{L}_H = G_2(\phi,X) - G_3(\phi,X)\Box\phi + G_4(\phi,X)R + G_{4,X}(\phi,X)[(\Box\phi)^2 - (\nabla_\mu\nabla_\nu\phi)(\nabla^\mu\nabla^\nu\phi)] + G_5(\phi,X)G_{\mu\nu}\nabla^\mu\nabla^\nu\phi$$
$$-\frac{1}{6}G_{5,X}(\phi,X)[(\Box\phi)^3 - 3(\Box\phi)(\nabla_\mu\nabla_\nu\phi)(\nabla^\mu\nabla^\nu\phi) + 2(\nabla^\mu\nabla_\alpha\phi)(\nabla^\alpha\nabla_\beta\phi)(\nabla^\beta\nabla_\mu\phi)], \tag{A2}$$

with $G_{\mu\nu}$ being the Einstein tensor. Four functions G_j ($j = 2, 3, 4, 5$) depend on the scalar field ϕ and its kinetic term $X = -g^{\mu\nu}\nabla_\mu\phi\nabla_\nu\phi/2$, where we use the notation $G_{j,X} \equiv \mathrm{d}G_j/\mathrm{d}X$. The action in Eq. (2.1) can be accommodated by the following coupling functions [105]:

$$G_2(\phi,X) = X - \frac{1}{4}\lambda\phi^4 + 8\mu^{(4)}(\phi)X^2(3 - \ln|X|), \tag{A3}$$

$$G_3(\phi,X) = 4\mu^{(3)}(\phi)X(7 - 3\ln|X|), \tag{A4}$$

$$G_4(\phi,X) = \frac{M_{\rm Pl}^2}{2} + \frac{1}{2}\xi\phi^2 + 4\mu^{(2)}(\phi)X(2 - \ln|X|), \tag{A5}$$

$$G_5(\phi,X) = -4\mu^{(1)}(\phi)\ln|X|, \tag{A6}$$

where $\mu^{(i)}(\phi) \equiv \mathrm{d}^i\mu/\mathrm{d}\phi^i$. In full Horndeski theories, the background and perturbation equations of motion on the flat FLRW background were already derived in Refs. [105,145,146]. In this paper, we applied those results to the theory given by the coupling functions (A3)–(A6).

[1] Y. B. Zel'dovich and I. D. Novikov, Sov. Astron. **10**, 602 (1967).
[2] S. Hawking, Mon. Not. R. Astron. Soc. **152**, 75 (1971).
[3] B. J. Carr and S. W. Hawking, Mon. Not. R. Astron. Soc. **168**, 399 (1974).
[4] G. F. Chapline, Nature (London) **253**, 251 (1975).
[5] P. Meszaros, Astron. Astrophys. **38**, 5 (1975).
[6] M. Y. Khlopov, Res. Astron. Astrophys. **10**, 495 (2010).
[7] M. Sasaki, T. Suyama, T. Tanaka, and S. Yokoyama, Classical Quantum Gravity **35**, 063001 (2018).
[8] B. Carr and F. Kuhnel, Annu. Rev. Nucl. Part. Sci. **70**, 355 (2020).
[9] A. M. Green and B. J. Kavanagh, J. Phys. G **48**, 043001 (2021).
[10] P. Villanueva-Domingo, O. Mena, and S. Palomares-Ruiz, Front. Astron. Space Sci. **8**, 87 (2021).
[11] B. Carr and F. Kuhnel, SciPost Phys. Lect. Notes **48**, 1 (2022).
[12] A. Escrivà, F. Kuhnel, and Y. Tada, arXiv:2211.05767.
[13] A. Karam, N. Koivunen, E. Tomberg, V. Vaskonen, and H. Veermäe, arXiv:2205.13540.
[14] B. P. Abbott *et al.* (LIGO Scientific, Virgo Collaborations), Phys. Rev. Lett. **116**, 061102 (2016).
[15] B. P. Abbott *et al.* (LIGO Scientific, Virgo Collaborations), Phys. Rev. X **9**, 031040 (2019).
[16] R. Abbott *et al.* (LIGO Scientific, Virgo Collaborations), Phys. Rev. X **11**, 021053 (2021).
[17] R. Abbott *et al.* (LIGO Scientific, Virgo, KAGRA Collaborations), arXiv:2111.03606.
[18] S. Bird, I. Cholis, J. B. Muñoz, Y. Ali-Haïmoud, M. Kamionkowski, E. D. Kovetz, A. Raccanelli, and A. G. Riess, Phys. Rev. Lett. **116**, 201301 (2016).
[19] M. Sasaki, T. Suyama, T. Tanaka, and S. Yokoyama, Phys. Rev. Lett. **117**, 061101 (2016); **121**, 059901(E) (2018).
[20] S. Clesse and J. García-Bellido, Phys. Dark Universe **15**, 142 (2017).
[21] S. Wang, Y.-F. Wang, Q.-G. Huang, and T. G. F. Li, Phys. Rev. Lett. **120**, 191102 (2018).
[22] R. Bean and J. Magueijo, Phys. Rev. D **66**, 063505 (2002).
[23] B. Carr, K. Kohri, Y. Sendouda, and J. Yokoyama, Rep. Prog. Phys. **84**, 116902 (2021).

[24] P. Ivanov, P. Naselsky, and I. Novikov, Phys. Rev. D **50**, 7173 (1994).
[25] J. Garcia-Bellido, A. D. Linde, and D. Wands, Phys. Rev. D **54**, 6040 (1996).
[26] J. S. Bullock and J. R. Primack, Phys. Rev. D **55**, 7423 (1997).
[27] J. Yokoyama, Astron. Astrophys. **318**, 673 (1997).
[28] J. Yokoyama, Phys. Rev. D **58**, 083510 (1998).
[29] M. Kawasaki, N. Sugiyama, and T. Yanagida, Phys. Rev. D **57**, 6050 (1998).
[30] M. Kawasaki, T. Takayama, M. Yamaguchi, and J. Yokoyama, Phys. Rev. D **74**, 043525 (2006).
[31] K. Kohri, D. H. Lyth, and A. Melchiorri, J. Cosmol. Astropart. Phys. 04 (2008) 038.
[32] R. Saito, J. Yokoyama, and R. Nagata, J. Cosmol. Astropart. Phys. 06 (2008) 024.
[33] E. Bugaev and P. Klimai, Phys. Rev. D **78**, 063515 (2008).
[34] L. Alabidi and K. Kohri, Phys. Rev. D **80**, 063511 (2009).
[35] M. Drees and E. Erfani, J. Cosmol. Astropart. Phys. 04 (2011) 005.
[36] M. Drees and E. Erfani, J. Cosmol. Astropart. Phys. 01 (2012) 035.
[37] J. Martin, H. Motohashi, and T. Suyama, Phys. Rev. D **87**, 023514 (2013).
[38] K. Kohri, C.-M. Lin, and T. Matsuda, Phys. Rev. D **87**, 103527 (2013).
[39] M. Kawasaki, N. Kitajima, and T. T. Yanagida, Phys. Rev. D **87**, 063519 (2013).
[40] S. Clesse and J. García-Bellido, Phys. Rev. D **92**, 023524 (2015).
[41] M. Kawasaki and Y. Tada, J. Cosmol. Astropart. Phys. 08 (2016) 041.
[42] M. Kawasaki, A. Kusenko, Y. Tada, and T. T. Yanagida, Phys. Rev. D **94**, 083523 (2016).
[43] S. Pi, Y.-l. Zhang, Q.-G. Huang, and M. Sasaki, J. Cosmol. Astropart. Phys. 05 (2018) 042.
[44] J. Garcia-Bellido and E. Ruiz Morales, Phys. Dark Universe **18**, 47 (2017).
[45] K. Kannike, L. Marzola, M. Raidal, and H. Veermäe, J. Cosmol. Astropart. Phys. 09 (2017) 020.
[46] C. Germani and T. Prokopec, Phys. Dark Universe **18**, 6 (2017).
[47] K. Ando, K. Inomata, M. Kawasaki, K. Mukaida, and T. T. Yanagida, Phys. Rev. D **97**, 123512 (2018).
[48] J. M. Ezquiaga, J. Garcia-Bellido, and E. Ruiz Morales, Phys. Lett. B **776**, 345 (2018).
[49] H. Motohashi and W. Hu, Phys. Rev. D **96**, 063503 (2017).
[50] H. Di and Y. Gong, J. Cosmol. Astropart. Phys. 07 (2018) 007.
[51] G. Ballesteros and M. Taoso, Phys. Rev. D **97**, 023501 (2018).
[52] J. Garcia-Bellido, M. Peloso, and C. Unal, J. Cosmol. Astropart. Phys. 09 (2017) 013.
[53] M. P. Hertzberg and M. Yamada, Phys. Rev. D **97**, 083509 (2018).
[54] K. Inomata, M. Kawasaki, K. Mukaida, and T. T. Yanagida, Phys. Rev. D **97**, 043514 (2018).
[55] Y.-F. Cai, X. Tong, D.-G. Wang, and S.-F. Yan, Phys. Rev. Lett. **121**, 081306 (2018).
[56] M. Drees and Y. Xu, Eur. Phys. J. C **81**, 182 (2021).
[57] V. Atal, J. Garriga, and A. Marcos-Caballero, J. Cosmol. Astropart. Phys. 09 (2019) 073.
[58] V. Atal, J. Cid, A. Escrivà, and J. Garriga, J. Cosmol. Astropart. Phys. 05 (2020) 022.
[59] S. S. Mishra and V. Sahni, J. Cosmol. Astropart. Phys. 04 (2020) 007.
[60] D. Y. Cheong, S. M. Lee, and S. C. Park, J. Cosmol. Astropart. Phys. 01 (2021) 032.
[61] C. Fu, P. Wu, and H. Yu, Phys. Rev. D **100**, 063532 (2019).
[62] I. Dalianis, S. Karydas, and E. Papantonopoulos, J. Cosmol. Astropart. Phys. 06 (2020) 040.
[63] A. Ashoorioon, A. Rostami, and J. T. Firouzjaee, J. High Energy Phys. 07 (2021) 087.
[64] J. Lin, Q. Gao, Y. Gong, Y. Lu, C. Zhang, and F. Zhang, Phys. Rev. D **101**, 103515 (2020).
[65] Z. Yi, Y. Gong, B. Wang, and Z.-h. Zhu, Phys. Rev. D **103**, 063535 (2021).
[66] G. A. Palma, S. Sypsas, and C. Zenteno, Phys. Rev. Lett. **125**, 121301 (2020).
[67] M. Braglia, D. K. Hazra, F. Finelli, G. F. Smoot, L. Sriramkumar, and A. A. Starobinsky, J. Cosmol. Astropart. Phys. 08 (2020) 001.
[68] K. Kefala, G. P. Kodaxis, I. D. Stamou, and N. Tetradis, Phys. Rev. D **104**, 023506 (2021).
[69] G. Ballesteros, J. Rey, M. Taoso, and A. Urbano, J. Cosmol. Astropart. Phys. 07 (2020) 025.
[70] Y. Aldabergenov, A. Addazi, and S. V. Ketov, Eur. Phys. J. C **80**, 917 (2020).
[71] Y. Aldabergenov, A. Addazi, and S. V. Ketov, Phys. Lett. B **814**, 136069 (2021).
[72] K. Inomata, E. McDonough, and W. Hu, Phys. Rev. D **104**, 123553 (2021).
[73] K. Inomata, E. McDonough, and W. Hu, J. Cosmol. Astropart. Phys. 02 (2022) 031.
[74] I. Dalianis, G. P. Kodaxis, I. D. Stamou, N. Tetradis, and A. Tsigkas-Kouvelis, Phys. Rev. D **104**, 103510 (2021).
[75] Y.-F. Cai, X.-H. Ma, M. Sasaki, D.-G. Wang, and Z. Zhou, Phys. Lett. B **834**, 137461 (2022).
[76] J. Lin, S. Gao, Y. Gong, Y. Lu, Z. Wang, and F. Zhang, Phys. Rev. D **107**, 043517 (2023).
[77] S. Kawai and J. Kim, Phys. Rev. D **104**, 083545 (2021).
[78] F. Zhang, Phys. Rev. D **105**, 063539 (2022).
[79] W. Ahmed, M. Junaid, and U. Zubair, Nucl. Phys. **B984**, 115968 (2022).
[80] Y.-F. Cai, X.-H. Ma, M. Sasaki, D.-G. Wang, and Z. Zhou, J. Cosmol. Astropart. Phys. 12 (2022) 034.
[81] S. Pi and J. Wang, arXiv:2209.14183.
[82] D. Y. Cheong, K. Kohri, and S. C. Park, J. Cosmol. Astropart. Phys. 10 (2022) 015.
[83] S. Kawai and J. Kim, arXiv:2209.15343.
[84] Y. Akrami *et al.* (Planck Collaboration), Astron. Astrophys. **641**, A10 (2020).
[85] A. M. Green and K. A. Malik, Phys. Rev. D **64**, 021301 (2001).
[86] B. A. Bassett and S. Tsujikawa, Phys. Rev. D **63**, 123503 (2001).
[87] T. Suyama, T. Tanaka, B. Bassett, and H. Kudoh, Phys. Rev. D **71**, 063507 (2005).

[88] J. Martin, T. Papanikolaou, and V. Vennin, J. Cosmol. Astropart. Phys. 01 (2020) 024.
[89] F. L. Bezrukov and M. Shaposhnikov, Phys. Lett. B **659**, 703 (2008).
[90] F. L. Bezrukov, A. Magnin, and M. Shaposhnikov, Phys. Lett. B **675**, 88 (2009).
[91] F. Bezrukov, A. Magnin, M. Shaposhnikov, and S. Sibiryakov, J. High Energy Phys. 01 (2011) 016.
[92] T. Futamase and K.-i. Maeda, Phys. Rev. D **39**, 399 (1989).
[93] R. Fakir and W. G. Unruh, Phys. Rev. D **41**, 1783 (1990).
[94] E. Komatsu and T. Futamase, Phys. Rev. D **59**, 064029 (1999).
[95] S. Tsujikawa and B. Gumjudpai, Phys. Rev. D **69**, 123523 (2004).
[96] A. Linde, M. Noorbala, and A. Westphal, J. Cosmol. Astropart. Phys. 03 (2011) 013.
[97] P. A. R. Ade *et al.* (Planck Collaboration), Astron. Astrophys. **571**, A22 (2014).
[98] S. Tsujikawa, J. Ohashi, S. Kuroyanagi, and A. De Felice, Phys. Rev. D **88**, 023529 (2013).
[99] J.-c. Hwang and H. Noh, Phys. Rev. D **71**, 063536 (2005).
[100] Z.-K. Guo, N. Ohta, and S. Tsujikawa, Phys. Rev. D **75**, 023520 (2007).
[101] M. Satoh and J. Soda, J. Cosmol. Astropart. Phys. 09 (2008) 019.
[102] Z.-K. Guo and D. J. Schwarz, Phys. Rev. D **80**, 063523 (2009).
[103] Z.-K. Guo and D. J. Schwarz, Phys. Rev. D **81**, 123520 (2010).
[104] S. Kawai and J. Kim, Phys. Rev. D **104**, 043525 (2021).
[105] T. Kobayashi, M. Yamaguchi, and J. Yokoyama, Prog. Theor. Phys. **126**, 511 (2011).
[106] R. Kase and S. Tsujikawa, Int. J. Mod. Phys. D **28**, 1942005 (2019).
[107] D. S. Salopek, J. R. Bond, and J. M. Bardeen, Phys. Rev. D **40**, 1753 (1989).
[108] N. Makino and M. Sasaki, Prog. Theor. Phys. **86**, 103 (1991).
[109] D. I. Kaiser, Phys. Rev. D **52**, 4295 (1995).
[110] A. De Simone, M. P. Hertzberg, and F. Wilczek, Phys. Lett. B **678**, 1 (2009).
[111] Y. Hamada, H. Kawai, K.-y. Oda, and S. C. Park, Phys. Rev. Lett. **112**, 241301 (2014).
[112] Y. Hamada, H. Kawai, K.-y. Oda, and S. C. Park, Phys. Rev. D **91**, 053008 (2015).
[113] F. Bezrukov, J. Rubio, and M. Shaposhnikov, Phys. Rev. D **92**, 083512 (2015).
[114] F. Bezrukov, M. Pauly, and J. Rubio, J. Cosmol. Astropart. Phys. 02 (2018) 040.
[115] G. W. Horndeski, Int. J. Theor. Phys. **10**, 363 (1974).
[116] C. Deffayet, X. Gao, D. A. Steer, and G. Zahariade, Phys. Rev. D **84**, 064039 (2011).
[117] C. Charmousis, E. J. Copeland, A. Padilla, and P. M. Saffin, Phys. Rev. Lett. **108**, 051101 (2012).
[118] A. De Felice and S. Tsujikawa, J. Cosmol. Astropart. Phys. 04 (2011) 029.
[119] D. J. Gross and J. H. Sloan, Nucl. Phys. **B291**, 41 (1987).
[120] R. R. Metsaev and A. A. Tseytlin, Nucl. Phys. **B293**, 385 (1987).
[121] M. Gasperini, M. Maggiore, and G. Veneziano, Nucl. Phys. **B494**, 315 (1997).
[122] S. Kawai, M.-a. Sakagami, and J. Soda, Phys. Lett. B **437**, 284 (1998).
[123] C. Cartier, J.-c. Hwang, and E. J. Copeland, Phys. Rev. D **64**, 103504 (2001).
[124] G. Calcagni, S. Tsujikawa, and M. Sami, Classical Quantum Gravity **22**, 3977 (2005).
[125] H. A. Khan and Yogesh, Phys. Rev. D **105**, 063526 (2022).
[126] A. M. Green, A. R. Liddle, K. A. Malik, and M. Sasaki, Phys. Rev. D **70**, 041502 (2004).
[127] S. Young, C. T. Byrnes, and M. Sasaki, J. Cosmol. Astropart. Phys. 07 (2014) 045.
[128] T. Harada, C.-M. Yoo, and K. Kohri, Phys. Rev. D **88**, 084051 (2013); **89**, 029903(E) (2014).
[129] C. Germani and I. Musco, Phys. Rev. Lett. **122**, 141302 (2019).
[130] B. J. Carr, Astrophys. J. **201**, 1 (1975).
[131] B. J. Kavanagh, bradkav/pbhbounds: Release version (2019).
[132] https://github.com/bradkav/PBHbounds/blob/master/bounds/README.md.
[133] K. Kohri and T. Terada, Phys. Rev. D **97**, 123532 (2018).
[134] T. Papanikolaou, V. Vennin, and D. Langlois, J. Cosmol. Astropart. Phys. 03 (2021) 053.
[135] M. H. Namjoo, H. Firouzjahi, and M. Sasaki, Europhys. Lett. **101**, 39001 (2013).
[136] G. Franciolini, A. Kehagias, S. Matarrese, and A. Riotto, J. Cosmol. Astropart. Phys. 03 (2018) 016.
[137] Y.-F. Cai, X. Chen, M. H. Namjoo, M. Sasaki, D.-G. Wang, and Z. Wang, J. Cosmol. Astropart. Phys. 05 (2018) 012.
[138] V. Atal and C. Germani, Phys. Dark Universe **24**, 100275 (2019).
[139] S. Passaglia, W. Hu, and H. Motohashi, Phys. Rev. D **99**, 043536 (2019).
[140] M. Taoso and A. Urbano, J. Cosmol. Astropart. Phys. 08 (2021) 016.
[141] M. Biagetti, V. De Luca, G. Franciolini, A. Kehagias, and A. Riotto, Phys. Lett. B **820**, 136602 (2021).
[142] M. W. Davies, P. Carrilho, and D. J. Mulryne, J. Cosmol. Astropart. Phys. 06 (2022) 019.
[143] J. Kristiano and J. Yokoyama, arXiv:2211.03395.
[144] K. Inomata, M. Braglia, and X. Chen, arXiv:2211.02586.
[145] A. De Felice and S. Tsujikawa, Phys. Rev. D **84**, 083504 (2011).
[146] A. De Felice, T. Kobayashi, and S. Tsujikawa, Phys. Lett. B **706**, 123 (2011).